Effects of Coulomb and isospin symmetry breaking interactions on neutron-skin thickness

Tomoya Naito (内藤智也) ⓘ,[1,2,*] Gianluca Colò ⓘ,[3,4,5,†] Haozhao Liang (梁豪兆) ⓘ,[2,1,‡] Xavier Roca-Maza ⓘ,[4,5,§] and Hiroyuki Sagawa (佐川弘幸)[6,7,∥]

[1]*RIKEN Interdisciplinary Theoretical and Mathematical Sciences Program (iTHEMS), Wako 351-0198, Japan*
[2]*Department of Physics, Graduate School of Science, The University of Tokyo, Tokyo 113-0033, Japan*
[3]*Yukawa Institute for Theoretical Physics, Kyoto University, Kyoto 606-8502, Japan*
[4]*Dipartimento di Fisica, Università degli Studi di Milano, Via Celoria 16, 20133 Milano, Italy*
[5]*INFN, Sezione di Milano, Via Celoria 16, 20133 Milano, Italy*
[6]*Center for Mathematics and Physics, University of Aizu, Aizu-Wakamatsu 965-8560, Japan*
[7]*RIKEN Nishina Center, Wako 351-0198, Japan*

Both the Coulomb interaction and isospin symmetry breaking (ISB) parts of the nuclear interaction break the isospin symmetry in atomic nuclei. Effects of these two kinds of interaction on properties of atomic nuclei, especially the mass difference of mirror nuclei and the neutron-skin thickness of $N = Z$ and $N \neq Z$ nuclei, are discussed. It is found that corrections to the Hartree-Fock-Slater approximation for the Coulomb interaction negligibly affect the neutron-skin thickness, while the charge-symmetry breaking term originating from the strong interaction might affect it non-negligibly. According to our calculations, the ISB terms other than the Coulomb interaction affect the estimation of the density dependence of the symmetry energy, L, by about 0–12 MeV using the correlation with the neutron-skin thickness.

I. INTRODUCTION

The isospin invariance of strong interaction was first proposed by Heisenberg in 1932 [1]. If the isospin symmetry of the strong interaction is fully valid, the charge symmetry and the charge independence of nuclear interaction hold. Here, the former denotes the case that the proton-proton nuclear interaction v_{pp} is the same as the neutron-neutron interaction v_{nn}, and the latter denotes the case that the $T = 1$ channel of the proton-neutron nuclear interaction v_{pn} is identical to the average of v_{pp} and v_{nn} for each L, S, ... channel. However, the isospin symmetry of atomic nuclei is partially broken due to the isospin symmetry breaking (ISB) terms of nuclear interaction together with the Coulomb interaction. The charge-symmetry breaking (CSB) term of nuclear interaction originates from the mass difference of protons and neutrons and the π^0-η and ρ^0-ω meson-exchange processes, and the charge-independence breaking (CIB) term of nuclear interaction is mainly due to the mass difference between π^0 and $\pi^{\pm}$ [2]. These two terms are defined by

$$v_{\mathrm{CSB}} \equiv v_{nn} - v_{pp}, \tag{1a}$$

$$v_{\mathrm{CIB}} \equiv v_{pn} - \frac{v_{nn} + v_{pp}}{2}, \tag{1b}$$

respectively. Effects of the ISB terms of the nuclear interaction on the nuclear properties have been discussed [3–26], as well as impact on neutron-star mass-radius relation [27].

The Coulomb interaction affects properties of the nuclear structure, and breaks the isospin symmetry of the atomic nuclei [5,28]. The ISB terms of nuclear interaction and Coulomb interaction are of different origins. These effects are, in general, measured as a net effect, while the Coulomb interaction plays a major role. To disentangle these effects from the experimental data, it is necessary to understand which quantities are sensitive to the ISB or Coulomb interaction. Hence, sensitivity studies for the Coulomb and the ISB terms of nuclear interactions are indispensable.

Here, a key issue to discuss such sensitivity studies is the accuracy of the calculation, since the ISB terms of the nuclear interaction are only a tiny part of the whole. To evaluate the contribution of the Coulomb interaction to nuclear properties, recently, a high-accuracy treatment of the Coulomb interaction for nuclear structure calculations was developed [29–31]. In this series of works, the density gradient effect was considered for the Coulomb exchange energy density functional (EDF) using the generalized gradient approximation (GGA). On top of that, the proton and neutron electric form factors were taken into account self-consistently, and the vacuum polarization for the Coulomb interaction was considered.

The ISB terms of the nuclear interactions have also been included in the Skyrme EDF [32] in Refs. [22,33–35]. We discussed a possibility to determine the CSB strength of the Skyrme interaction referring to *ab initio* calculations [36].

---

*tnaito@ribf.riken.jp

†colo@mi.infn.it

‡haozhao.liang@phys.s.u-tokyo.ac.jp

§xavier.roca.maza@mi.infn.it

∥sagawa@ribf.riken.jp

This paper aims to a complete sensitivity study of the nuclear EoS and the neutron-skin thickness to the Coulomb and ISB terms. In the previous Letter [37], we discussed the effect of ISB terms on the charge-radii difference of mirror nuclei ΔR_{ch} and, accordingly, on estimating the density dependence of the symmetry energy, L, using ΔR_{ch}. In this paper, we will discuss similar analyses for different quantities related to isospin symmetry breaking: the neutron-skin thickness and the mass differences of mirror nuclei. The ISB effect on the difference between the calculated charge radius of ^{40}Ca and that of ^{48}Ca, where it was claimed that such difference is related to the symmetry energy of an employed EDF [38], will also be discussed.

This paper is organized as follows. In Sec. II, effects of the ISB terms on nuclear matter properties will be discussed. In Sec. III, the theoretical framework will be shown. In Sec. IV, the sensitivity study of the neutron-skin thickness ΔR_{np}, the difference between the charge radius of ^{40}Ca and that of ^{48}Ca,

and mass differences of mirror nuclei will be investigated. The ISB effect on the correlation between the neutron-skin thickness and the density dependence of the symmetry energy [39–41] will also be discussed. In Sec. V, we will summarize this paper.

II. ISOSPIN SYMMETRY BREAKING INTERACTION AND NUCLEAR EQUATION OF STATE

In this section, the ISB contributions to nuclear matter properties are discussed. In order to discuss it, first, the energy density of the Skyrme-ISB interaction is shown. Although only the leading-order (t_0-like) Skyrme-ISB interaction is considered in our numerical calculations, we will show the momentum-dependent (t_1 and t_2-like) Skyrme-ISB contributions for the EDF here.

The Skyrme CSB and CIB interactions are denoted by

$$v_{\mathrm{Sky}}^{\mathrm{CSB}}(\boldsymbol{r}) = \left\{ s_0(1 + y_0 P_\sigma)\delta(\boldsymbol{r}) + \frac{s_1}{2}(1 + y_1 P_\sigma)[\boldsymbol{k}^{\dagger 2}\delta(\boldsymbol{r}) + \delta(\boldsymbol{r})\boldsymbol{k}^2] + s_2(1 + y_2 P_\sigma)\boldsymbol{k}^\dagger \cdot \delta(\boldsymbol{r})\boldsymbol{k} \right\} \frac{\tau_{z1} + \tau_{z2}}{4}, \tag{2a}$$

$$v_{\mathrm{Sky}}^{\mathrm{CIB}}(\boldsymbol{r}) = \left\{ u_0(1 + z_0 P_\sigma)\delta(\boldsymbol{r}) + \frac{u_1}{2}(1 + z_1 P_\sigma)[\boldsymbol{k}^{\dagger 2}\delta(\boldsymbol{r}) + \delta(\boldsymbol{r})\boldsymbol{k}^2] + u_2(1 + z_2 P_\sigma)\boldsymbol{k}^\dagger \cdot \delta(\boldsymbol{r})\boldsymbol{k} \right\} (a_1 \boldsymbol{\tau}_1 \cdot \boldsymbol{\tau}_2 + a_2 \tau_{z1}\tau_{z2}), \tag{2b}$$

respectively, in analogy with the isospin-symmetric Skyrme interaction [32,42]

$$v_{\mathrm{Sky}}^{\mathrm{IS}}(\boldsymbol{r}) = t_0(1 + x_0 P_\sigma)\delta(\boldsymbol{r}) + \frac{t_1}{2}(1 + x_1 P_\sigma)[\boldsymbol{k}^{\dagger 2}\delta(\boldsymbol{r}) + \delta(\boldsymbol{r})\boldsymbol{k}^2] + t_2(1 + x_2 P_\sigma)\boldsymbol{k}^\dagger \cdot \delta(\boldsymbol{r})\boldsymbol{k}$$
$$+ \frac{t_3}{6}(1 + x_3 P_\sigma)\delta(\boldsymbol{r})[\rho(\boldsymbol{R})]^\alpha + iW_0 \boldsymbol{\sigma} \cdot \boldsymbol{k}^\dagger \times \delta(\boldsymbol{r})\boldsymbol{k}, \tag{3}$$

where $\boldsymbol{r} = \boldsymbol{r}_1 - \boldsymbol{r}_2$ and $\boldsymbol{R} = (\boldsymbol{r}_1 + \boldsymbol{r}_2)/2$. See Ref. [43] for the standard definitions of the other symbols.

It is worthwhile to discuss the form of the CIB operator. Three types of the CIB operator—the simple form $\tau_{z1}\tau_{z2}$, the isotensor form $T_{12} = \boldsymbol{\tau}_1 \cdot \boldsymbol{\tau}_2 - 3\tau_{z1}\tau_{z2}$, and the general form $a_1 \boldsymbol{\tau}_1 \cdot \boldsymbol{\tau}_2 + a_2 \tau_{z1}\tau_{z2}$—are widely used [7,22,33,44]. However, there is no criterion to fix values of a_1 and a_2 in $a_1 \boldsymbol{\tau}_1 \cdot \boldsymbol{\tau}_2 + a_2 \tau_{z1}\tau_{z2}$ from any fundamental theory. For example, as shown in Appendix A, according to the one-pion exchange nuclear interaction, a relation $a_1 = -a_2$ can be derived; however, the one-pion exchange interaction gives only a part of the CIB interaction. The difference between the isotensor and the one-pion exchange forms can be absorbed in the isospin symmetric part, i.e., the term $\boldsymbol{\tau}_1 \cdot \boldsymbol{\tau}_2$ itself is isospin symmetric. In order to keep generality, here, the general form of CIB operator, $a_1 \boldsymbol{\tau}_1 \cdot \boldsymbol{\tau}_2 + a_2 \tau_{z1}\tau_{z2}$, is adopted.

It will be shown that if one uses $a_1 = -a_2$ for the CIB operator and does not assume the formalism of the proton-neutron mixed density functional theory [45–47], the CIB contributions to the energy density vanishes.[1] For other cases,

whatever form of CIB operator is used, the CIB contribution to the nuclear matter does not vanish. Therefore, whichever form of the CIB operator other than $a_1 = -a_2$ is used, there is neither disadvantage nor advantage. Note that the ISB contributions to the energy density in the formalism of the proton-neutron mixed density functional theory is given in Ref. [48].

A. ISB nuclear energy density

Although the ISB nuclear energy density has been shown in Ref. [49], it is convenient to show it here again to discuss effects of ISB terms on nuclear matter properties. The nuclear energy density for the isospin symmetric part is shown in, for example, Refs. [32,45,50,51]. Here, we do not consider the proton-neutron mixed density, i.e., $\rho_{pn}(\boldsymbol{r})$ and $\rho_{np}(\boldsymbol{r})$ are assumed to be zero.

Using the expectation values of the CSB and CIB operators, expanding the wave function on a basis where the $\boldsymbol{\tau}$ and τ_z are good quantum numbers, one obtains

$$\langle pp|\boldsymbol{\tau}_1 \cdot \boldsymbol{\tau}_2|pp\rangle = \langle nn|\boldsymbol{\tau}_1 \cdot \boldsymbol{\tau}_2|nn\rangle = 1, \tag{4a}$$

$$\langle pn|\boldsymbol{\tau}_1 \cdot \boldsymbol{\tau}_2|pn\rangle = \langle np|\boldsymbol{\tau}_1 \cdot \boldsymbol{\tau}_2|np\rangle = -1, \tag{4b}$$

$$\langle pn|\boldsymbol{\tau}_1 \cdot \boldsymbol{\tau}_2|np\rangle = 2. \tag{4c}$$

---

[1]This is true even if one takes a Gogny interaction.

Accordingly, we get

$$
\mathcal{E}_{\text{CSB}}^{\text{H}} = \frac{s_0}{4}\left(1 + \frac{y_0}{2}\right)(\rho_n^2 - \rho_p^2) + \frac{1}{8}\left[s_1\left(1 + \frac{y_1}{2}\right) + s_2\left(1 + \frac{y_2}{2}\right)\right](\rho_n t_n - \rho_p t_p)
$$
$$
- \frac{1}{32}\left[3s_1\left(1 + \frac{y_1}{2}\right) - s_2\left(1 + \frac{y_2}{2}\right)\right](\rho_n \Delta\rho_n - \rho_p \Delta\rho_p) - \frac{1}{32}(s_1 y_1 + s_2 y_2)\left(\boldsymbol{J}_n^2 - \boldsymbol{J}_p^2\right), \tag{5a}
$$

$$
\mathcal{E}_{\text{CSB}}^{\text{x}} = -\frac{s_0}{4}\left(\frac{1}{2} + y_0\right)(\rho_n^2 - \rho_p^2) - \frac{1}{8}\left[s_1\left(\frac{1}{2} + y_1\right) - s_2\left(\frac{1}{2} + y_2\right)\right](\rho_n t_n - \rho_p t_p)
$$
$$
+ \frac{1}{32}\left[3s_1\left(\frac{1}{2} + y_1\right) + s_2\left(\frac{1}{2} + y_2\right)\right](\rho_n \Delta\rho_n - \rho_p \Delta\rho_p) + \frac{1}{32}(s_1 - s_2)\left(\boldsymbol{J}_n^2 - \boldsymbol{J}_p^2\right), \tag{5b}
$$

$$
\mathcal{E}_{\text{CIB}}^{\text{H}} = (a_1 + a_2)\left\{\frac{u_0}{2}\left(1 + \frac{z_0}{2}\right)(\rho_n - \rho_p)^2 + \frac{1}{4}\left[u_1\left(1 + \frac{z_1}{2}\right) + u_2\left(1 + \frac{z_2}{2}\right)\right](\rho_n - \rho_p)(t_n - t_p)\right.
$$
$$
\left. - \frac{1}{16}\left[3u_1\left(1 + \frac{z_1}{2}\right) - u_2\left(1 + \frac{z_2}{2}\right)\right](\rho_n - \rho_p)(\Delta\rho_n - \Delta\rho_p) - \frac{1}{16}(u_1 z_1 + u_2 z_2)(\boldsymbol{J}_n - \boldsymbol{J}_p)^2\right\} \tag{5c}
$$

$$
\mathcal{E}_{\text{CIB}}^{\text{x}} = (a_1 + a_2)\left\{-\frac{u_0}{2}\left(\frac{1}{2} + z_0\right)(\rho_n^2 + \rho_p^2) - \frac{1}{4}\left[u_1\left(\frac{1}{2} + z_1\right) - u_2\left(\frac{1}{2} + z_2\right)\right](\rho_n t_n + \rho_p t_p)\right.
$$
$$
\left. + \frac{1}{16}\left[3u_1\left(\frac{1}{2} + z_1\right) + u_2\left(\frac{1}{2} + z_2\right)\right](\rho_n \Delta\rho_n + \rho_p \Delta\rho_p) + \frac{1}{16}(u_1 - u_2)\left(\boldsymbol{J}_n^2 + \boldsymbol{J}_p^2\right)\right\}, \tag{5d}
$$

where $t_\tau = \sum_j |\nabla\varphi_{j\tau}|^2$ and $\boldsymbol{J}_\tau = \sum_j \varphi_{j\tau}\boldsymbol{\sigma} \times \nabla\varphi_{j\tau}$ are the kinetic energy and spin-orbit densities for nucleon of species τ, and $\mathcal{E}^{\text{H}}$ and $\mathcal{E}^{\text{x}}$ correspond to the Hartree and exchange contributions, respectively.

B. Nuclear equation of state with ISB terms

The nuclear equation of state can be calculated as

$$
\frac{E_{\text{Skyrme}}}{A}(\rho, \beta) = \varepsilon_{\text{Skyrme}}(\rho, \beta)
$$
$$
= \varepsilon_0(\rho) + \varepsilon_1(\rho)\beta + \varepsilon_2(\rho)\beta^2 + O(\beta^3), \tag{6a}
$$

$$
\varepsilon_0(\rho) = \frac{3}{5}\frac{\hbar^2}{2m}\left(\frac{3\pi^2}{2}\right)^{2/3}\rho^{2/3} + \frac{1}{8}[3t_0 - (a_1 + a_2)u_0(1 + 2z_0)]\rho
$$
$$
+ \frac{3}{80}\left(\frac{3\pi^2}{2}\right)^{2/3}\{3t_1 + t_2(5 + 4x_2) - (a_1 + a_2)[u_1(1 + 2z_1) - u_2(1 + 2z_2)]\}\rho^{5/3} + \frac{t_3}{16}\rho^{\alpha+1}, \tag{6b}
$$

$$
\varepsilon_1(\beta) = \frac{s_0}{8}(1 - y_0)\rho + \frac{1}{20}\left(\frac{3\pi^2}{2}\right)^{2/3}[s_1(1 - y_1) + 3s_2(1 + y_2)]\rho^{5/3}, \tag{6c}
$$

$$
\varepsilon_2(\beta) = \frac{1}{3}\frac{\hbar^2}{2m}\left(\frac{3\pi^2}{2}\right)^{2/3}\rho^{2/3} - \frac{1}{8}[t_0(1 + 2x_0) - 3(a_1 + a_2)u_0]\rho
$$
$$
- \frac{1}{24}\left(\frac{3\pi^2}{2}\right)^{2/3}\{3t_1 x_1 - t_2(4 + 5x_2) - (a_1 + a_2)[u_1(4 - z_1) + u_2(8 + 7z_2)]\}\rho^{5/3} - \frac{t_3}{48}(1 + 2x_3)\rho^{\alpha+1}, \tag{6d}
$$

where $\rho = \rho_n + \rho_p$ and $\beta = (\rho_n - \rho_p)/\rho$. It is obviously found that the CIB term contributes to the isoscalar term and β^2 term, while the CSB term generates β term. Here, E_{Skyrme} is the Skyrme EDF, which also includes the CSB and CIB contributions [Eq. (5)], as well as the ordinary isospin symmetric part.

If one does not consider the CSB term, $\varepsilon_1 \equiv 0$ holds; accordingly, the symmetry energy ε_{sym} can be simply defined by $\varepsilon_{\text{sym}}(\rho) = \varepsilon_2(\rho)$, which is the usual definition. Once the CSB term is introduced, ε_1 term appears and there can be several possible definitions of ε_{sym}: ε_{sym} is defined by $\varepsilon_{\text{sym}}(\rho) = \frac{1}{2}\frac{\partial^2\varepsilon(\rho,\beta)}{\partial\beta^2}|_{\beta=0}$ or by $\varepsilon_{\text{sym}}(\rho) = \varepsilon(\rho, 1) - \varepsilon(\rho, 0)$. As discussed in Ref. [37], the latter definition

$$
\varepsilon_{\text{sym}}(\rho) = \varepsilon(\rho, 1) - \varepsilon(\rho, 0)
$$
$$
\simeq \varepsilon_1(\rho) + \varepsilon_2(\rho) \tag{7}
$$

leads to the straightforward extension of the relation between the pressure of neutron matter at the saturation density, $P(\rho_{\text{sat}}, 1)$, and the density dependence of symmetry energy,

L, as $P(\rho_{\text{sat}}, 1) = L\rho_{\text{sat}}/3$. The approximation of Eq. (7) is justified around the saturation density since the terms higher order than β^2 are small.

EoS parameters ε_{sat}, K_{∞}, J, L, and K_{sym} and their extensions to ISB terms are defined by [52]

$$\varepsilon_0(\rho) = \varepsilon_{\text{sat}} + \varepsilon_{\text{sat}}^{\text{CIB}} + \frac{1}{2}\left(K_{\infty} + K_{\infty}^{\text{CIB}}\right)\left(\frac{\rho - \rho_{\text{sat}}}{3\rho_{\text{sat}}}\right)^2 + \dots, \tag{8a}$$

$$\varepsilon_{\text{sym}}(\rho) = \left(J + J^{\text{CIB}} + J^{\text{CSB}}\right) + \left(L + L^{\text{CIB}} + L^{\text{CSB}}\right)\left(\frac{\rho - \rho_{\text{sat}}}{3\rho_{\text{sat}}}\right) + \frac{1}{2}\left(K_{\text{sym}} + K_{\text{sym}}^{\text{CIB}} + K_{\text{sym}}^{\text{CSB}}\right)\left(\frac{\rho - \rho_{\text{sat}}}{3\rho_{\text{sat}}}\right)^2 + \dots, \tag{8b}$$

where the CSB contribution to ε_{sat} and K_{∞} are zero. These EoS parameters read

$$\varepsilon_{\text{sat}} = \frac{3}{5}\frac{\hbar^2}{2m}\left(\frac{3\pi^2}{2}\right)^{2/3}\rho_{\text{sat}}^{2/3} + \frac{3}{8}t_0\rho_{\text{sat}} + \frac{3}{80}\left(\frac{3\pi^2}{2}\right)^{2/3}[3t_1 + t_2(5 + 4x_2)]\rho_{\text{sat}}^{5/3} + \frac{t_3}{16}\rho_{\text{sat}}^{\alpha+1}, \tag{9a}$$

$$\varepsilon_{\text{sat}}^{\text{CIB}} = -\frac{1}{8}(a_1 + a_2)u_0(1 + 2z_0)\rho_{\text{sat}} - \frac{3}{80}\left(\frac{3\pi^2}{2}\right)^{2/3}(a_1 + a_2)[u_1(1 + 2z_1) - u_2(1 + 2z_2)]\rho_{\text{sat}}^{5/3}, \tag{9b}$$

$$K_{\infty} = -\frac{6}{5}\frac{\hbar^2}{2m}\left(\frac{3\pi^2}{2}\right)^{2/3}\rho_{\text{sat}}^{2/3} + \frac{3}{8}\left(\frac{3\pi^2}{2}\right)^{2/3}[3t_1 + t_2(5 + 4x_2)]\rho_{\text{sat}}^{5/3} + \frac{9}{16}t_3\alpha(\alpha + 1)\rho_{\text{sat}}^{\alpha+1}, \tag{9c}$$

$$K_{\infty}^{\text{CIB}} = -\frac{3}{8}\left(\frac{3\pi^2}{2}\right)^{2/3}(a_1 + a_2)[u_1(1 + 2z_1) - u_2(1 + 2z_2)]\rho_{\text{sat}}^{5/3}, \tag{9d}$$

$$J = \frac{1}{3}\frac{\hbar^2}{2m}\left(\frac{3\pi^2}{2}\right)^{2/3}\rho_{\text{sat}}^{2/3} - \frac{t_0}{8}(1 + 2x_0)\rho_{\text{sat}} - \frac{1}{24}\left(\frac{3\pi^2}{2}\right)^{2/3}[3t_1x_1 - t_2(4 + 5x_2)]\rho_{\text{sat}}^{5/3} - \frac{t_3}{48}(1 + 2x_3)\rho_{\text{sat}}^{\alpha+1}, \tag{9e}$$

$$J^{\text{CIB}} = \frac{3}{8}(a_1 + a_2)u_0\rho_{\text{sat}} + \frac{1}{24}\left(\frac{3\pi^2}{2}\right)^{2/3}(a_1 + a_2)[u_1(4 - z_1) + u_2(8 + 7z_2)]\rho_{\text{sat}}^{5/3}, \tag{9f}$$

$$J^{\text{CSB}} = \frac{s_0}{8}(1 - y_0)\rho_{\text{sat}} + \frac{1}{20}\left(\frac{3\pi^2}{2}\right)^{2/3}[s_1(1 - y_1) + 3s_2(1 + y_2)]\rho_{\text{sat}}^{5/3}, \tag{9g}$$

$$L = \frac{2}{3}\frac{\hbar^2}{2m}\left(\frac{3\pi^2}{2}\right)^{2/3}\rho_{\text{sat}}^{2/3} - \frac{3}{8}t_0(1 + 2x_0)\rho_{\text{sat}} - \frac{5}{24}\left(\frac{3\pi^2}{2}\right)^{2/3}[3t_1x_1 - t_2(4 + 5x_2)]\rho_{\text{sat}}^{5/3} - \frac{t_3}{16}(1 + 2x_3)(\alpha + 1)\rho_{\text{sat}}^{\alpha+1}, \tag{9h}$$

$$L^{\text{CIB}} = \frac{9}{8}(a_1 + a_2)u_0\rho_{\text{sat}} + \frac{5}{24}\left(\frac{3\pi^2}{2}\right)^{2/3}(a_1 + a_2)[u_1(4 - z_1) + u_2(8 + 7z_2)]\rho_{\text{sat}}^{5/3}, \tag{9i}$$

$$L^{\text{CSB}} = \frac{3}{8}s_0(1 - y_0)\rho_{\text{sat}} + \frac{1}{4}\left(\frac{3\pi^2}{2}\right)^{2/3}[s_1(1 - y_1) + 3s_2(1 + y_2)]\rho_{\text{sat}}^{5/3}, \tag{9j}$$

$$K_{\text{sym}} = -\frac{2}{3}\frac{\hbar^2}{2m}\left(\frac{3\pi^2}{2}\right)^{2/3}\rho_{\text{sat}}^{2/3} - \frac{5}{12}\left(\frac{3\pi^2}{2}\right)^{2/3}[3t_1x_1 - t_2(4 + 5x_2)]\rho_{\text{sat}}^{5/3} - \frac{3}{16}t_3(1 + 2x_3)\alpha(\alpha + 1)\rho_{\text{sat}}^{\alpha+1}, \tag{9k}$$

$$K_{\text{sym}}^{\text{CIB}} = \frac{5}{12}\left(\frac{3\pi^2}{2}\right)^{2/3}(a_1 + a_2)[u_1(4 - z_1) + u_2(8 + 7z_2)]\rho_{\text{sat}}^{5/3}, \tag{9l}$$

$$K_{\text{sym}}^{\text{CSB}} = \frac{1}{2}\left(\frac{3\pi^2}{2}\right)^{2/3}[s_1(1 - y_1) + 3s_2(1 + y_2)]\rho_{\text{sat}}^{5/3}, \tag{9m}$$

respectively.

The pressure of nuclear matter reads

$$
\begin{aligned}
P(\rho, \beta) &= \rho^2 \frac{\partial \varepsilon_{\text{Skyrme}}(\rho, \beta)}{\partial \rho} \\
&\simeq \left\{ \frac{2}{5} \frac{\hbar^2}{2m} \left(\frac{3\pi^2}{2} \right)^{2/3} \rho^{5/3} + \frac{1}{8} [3t_0 - (a_1 + a_2)u_0(1 + 2z_0)]\rho^2 \right. \\
&\quad \left. + \frac{1}{16} \left(\frac{3\pi^2}{2} \right)^{2/3} \{3t_1 + t_2(5 + 4x_2) - (a_1 + a_2)[u_1(1 + 2z_1) - u_2(1 + 2z_2)]\}\rho^{8/3} + \frac{t_3}{16}(\alpha + 1)\rho^{\alpha+2} \right\} \\
&\quad + \left\{ \frac{s_0}{8}(1 - y_0)\rho^2 + \frac{1}{12}\left(\frac{3\pi^2}{2} \right)^{2/3} [s_1(1 - y_1) + 3s_2(1 + y_2)]\rho^{8/3} \right\} \beta \\
&\quad + \left\{ \frac{2}{9} \frac{\hbar^2}{2m} \left(\frac{3\pi^2}{2} \right)^{2/3} \rho^{5/3} - \frac{1}{8}[t_0(1 + 2x_0) - 3(a_1 + a_2)u_0]\rho^2 - \frac{5}{72}\left(\frac{3\pi^2}{2} \right)^{2/3} \right. \\
&\quad \left. \times \{3t_1x_1 - t_2(4 + 5x_2) - (a_1 + a_2)[u_1(4 - z_1) + u_2(8 + 7z_2)]\}\rho^{8/3} - \frac{t_3}{48}(\alpha + 1)(1 + 2x_3)\rho^{\alpha+2} \right\}\beta^2,
\end{aligned}
\tag{10}
$$

where the higher-order terms than β^2 are neglected. The pressure of the pure neutron matter at the saturation density reads

$$
\begin{aligned}
P(\rho_{\text{sat}}, 1) &\simeq \left\{ \frac{s_0}{8}(1 - y_0)\rho_{\text{sat}}^2 + \frac{1}{12}\left(\frac{3\pi^2}{2} \right)^{2/3} [s_1(1 - y_1) + 3s_2(1 + y_2)]\rho_{\text{sat}}^{8/3} \right\} \\
&\quad + \left\{ \frac{2}{9} \frac{\hbar^2}{2m} \left(\frac{3\pi^2}{2} \right)^{2/3} \rho_{\text{sat}}^{5/3} - \frac{1}{8}[t_0(1 + 2x_0) - 3(a_1 + a_2)u_0]\rho_{\text{sat}}^2 - \frac{5}{72}\left(\frac{3\pi^2}{2} \right)^{2/3} \right. \\
&\quad \left. \times \{3t_1x_1 - t_2(4 + 5x_2) - (a_1 + a_2)[u_1(4 - z_1) + u_2(8 + 7z_2)]\}\rho_{\text{sat}}^{8/3} - \frac{t_3}{48}(\alpha + 1)(1 + 2x_3)\rho_{\text{sat}}^{\alpha+2} \right\} \\
&= \frac{L + L^{\text{CIB}} + L^{\text{CSB}}}{3}\rho_{\text{sat}}.
\end{aligned}
\tag{11}
$$

The saturation density ρ_{sat}, which is defined by $P(\rho_{\text{sat}}, 0) = 0$, satisfies

$$
\begin{aligned}
&\frac{2}{5} \frac{\hbar^2}{2m} \left(\frac{3\pi^2}{2} \right)^{2/3} \rho_{\text{sat}}^{5/3} + \frac{1}{8}[3t_0 - (a_1 + a_2)u_0(1 + 2z_0)]\rho_{\text{sat}}^2 + \frac{1}{16}\left(\frac{3\pi^2}{2} \right)^{2/3} \\
&\quad \times \{3t_1 + t_2(5 + 4x_2) - (a_1 + a_2)[u_1(1 + 2z_1) - u_2(1 + 2z_2)]\}\rho_{\text{sat}}^{8/3} + \frac{t_3}{16}(\alpha + 1)\rho_{\text{sat}}^{\alpha+2} \simeq 0,
\end{aligned}
\tag{12}
$$

where the approximation comes from Eq. (10) and is correct up to β^2. This equation implies that the saturation density ρ_{sat} itself is changed due to the CIB term. Effects of ISB terms to the saturation density and EoS parameters are discussed in Sec. IV A.

III. EDFS OF ISB AND COULOMB INTERACTIONS

To calculate the density and total energy, the self-consistent nuclear density functional theory [53–58] is used. In nuclear density functional theory including the case of Skyrme EDFs, the ground-state energy is written as

$$
\begin{aligned}
E_{\text{gs}} = T_0 &+ E_{\text{IS}}[\rho_p, \rho_n] + E_{\text{CSB}}[\rho_p, \rho_n] \\
&+ E_{\text{CIB}}[\rho_p, \rho_n] + E_{\text{Coul}}[\rho_{\text{ch}}],
\end{aligned}
\tag{13}
$$

where T_0, E_{IS}, E_{CSB}, E_{CIB}, and E_{Coul} are the Kohn-Sham kinetic energy, the isospin symmetric, CSB, CIB, and the Coulomb EDFs, respectively. The proton and neutron density distribution are denoted by ρ_p and ρ_n, respectively. The defi-

nition of the charge density distribution ρ_{ch} will be discussed in the next section.

A. Nuclear part

In SHF, the isospin symmetric nuclear term E_{IS} is the standard Skyrme EDF [32,50]. In this paper, we mainly use the SAMi EDF [59] and the SAMi-J EDF family [60]. In addition, we also use the SAMi-ISB EDF [22]. Note that the SAMi-ISB EDF includes E_{CSB} and E_{CIB} as well; we call the SAMi-ISB EDF without ISB terms, as the "SAMi-noISB" EDF to avoid any confusion with the SAMi EDF without ISB terms. The E_{IS} of SAMi-noISB EDF is different from that of the original SAMi EDF, since E_{IS}, E_{CSB}, and E_{CIB} are optimized altogether simultaneously, although the same protocol was adopted. In the original papers of these EDFs [22,59], only limited digits are shown. However, since we will discuss details of numerical results, more digits are demanded

to achieve higher accuracy. The precise values of the parameters of SAMi and SAMi-ISB EDFs are shown in Appendix B.

For the ISB terms of nuclear part, E_{CSB} and E_{CIB}, we adopt the SAMi-ISB EDF, whose forms are the leading-order Skyrme-ISB interaction, i.e., $s_1 = s_2 = u_1 = u_2 = 0$ in Eqs. (2), with $a_1 = 0$ and $a_2 = 1/2$. The CSB and CIB EDFs, respectively, read

$$E_{\text{CSB}}[\rho_p, \rho_n] = \frac{s_0(1 - y_0)}{8} \int \{[\rho_n(\boldsymbol{r})]^2 - [\rho_p(\boldsymbol{r})]^2\}\, d\boldsymbol{r}, \quad (14)$$

$$\begin{aligned} E_{\text{CIB}}[\rho_p, \rho_n] &= \frac{u_0(1 - z_0)}{8} \int \{[\rho_n(\boldsymbol{r})]^2 + [\rho_p(\boldsymbol{r})]^2\}\, d\boldsymbol{r} \\ &\quad - \frac{u_0(2 + z_0)}{4} \int \rho_n(\boldsymbol{r})\rho_p(\boldsymbol{r})\, d\boldsymbol{r} \end{aligned} \quad (15)$$

with $y_0 = z_0 = -1$.

B. Coulomb part

The Coulomb part E_{Coul} is, in general, divided into four terms, the Coulomb Hartree term E_{CH}, the Coulomb exchange term E_{Cx}, the vacuum polarization term E_{VP}, and the electromagnetic spin-orbit term E_{EMSO} [31]. Note that many-body effects of the Coulomb interaction, namely, the Coulomb correlation [29,61–63], are not considered in this paper and left for future perspectives. We start from the Hartree-Fock-Slater approximation [64,65], i.e., the Coulomb LDA exchange EDF for E_{Cx} with $E_{\text{VP}} \equiv 0$ and $E_{\text{EMSO}} \equiv 0$, together with the point-particle approximation $\rho_{\text{ch}} \equiv \rho_p$. On top of the Hartree-Fock-Slater approximation, in order to see effects of the Coulomb interaction, the precise treatment of the Coulomb interaction—the GGA, the proton finite-size effect, the neutron finite-size effect, and the vacuum polarization E_{VP}—is introduced step by step as proposed in Ref. [31]. We use abbreviations "NoEx," "LDA," "GGA," "*p*-fin," "*pn*-fin," and "All" for

$$E_{\text{Coul}}^{\text{NoEx}} = E_{\text{CH}}[\rho_p], \quad (16a)$$

$$E_{\text{Coul}}^{\text{LDA}} = E_{\text{CH}}[\rho_p] + E_{\text{Cx}}^{\text{LDA}}[\rho_p], \quad (16b)$$

$$E_{\text{Coul}}^{\text{GGA}} = E_{\text{CH}}[\rho_p] + E_{\text{Cx}}^{\text{GGA}}[\rho_p], \quad (16c)$$

$$E_{\text{Coul}}^{p\text{-fin}} = E_{\text{CH}}[\rho_{\text{ch}}^{p\text{-fin}}] + E_{\text{Cx}}^{\text{GGA}}[\rho_{\text{ch}}^{p\text{-fin}}], \quad (16d)$$

$$E_{\text{Coul}}^{pn\text{-fin}} = E_{\text{CH}}[\rho_{\text{ch}}^{pn\text{-fin}}] + E_{\text{Cx}}^{\text{GGA}}[\rho_{\text{ch}}^{pn\text{-fin}}], \quad (16e)$$

$$E_{\text{Coul}}^{\text{All}} = E_{\text{CH}}[\rho_{\text{ch}}^{pn\text{-fin}}] + E_{\text{Cx}}^{\text{GGA}}[\rho_{\text{ch}}^{pn\text{-fin}}] + E_{\text{VP}}[\rho_p], \quad (16f)$$

respectively. Here, $E_{\text{Cx}}^{\text{LDA}}$ and $E_{\text{Cx}}^{\text{GGA}}$ are the Coulomb exchange EDFs in the LDA and GGA,

$$E_{\text{Cx}}^{\text{LDA}}[\rho] = -\frac{3e^2}{4}\left(\frac{3}{\pi}\right)^{1/3} \int [\rho(\boldsymbol{r})]^{4/3}\, d\boldsymbol{r}, \quad (17a)$$

$$E_{\text{Cx}}^{\text{GGA}}[\rho] = -\frac{3e^2}{4}\left(\frac{3}{\pi}\right)^{1/3} \int F(s(\boldsymbol{r}))[\rho(\boldsymbol{r})]^{4/3}\, d\boldsymbol{r}, \quad (17b)$$

respectively. In this paper, we use the modified Perdew-Burke-Ernzerhof GGA enhancement factor [66]

$$F(s) = 1 + \kappa - \frac{\kappa}{1 + \lambda \mu s^2 / \kappa}, \quad (18a)$$

$$s = \frac{|\boldsymbol{\nabla}\rho|}{2k_{\text{F}}\rho}, \quad (18b)$$

$$k_{\text{F}} = (3\pi^2\rho)^{1/3}, \quad (18c)$$

$$\mu = 0.21951, \quad (18d)$$

$$\kappa = 0.804, \quad (18e)$$

with $\lambda = 1.25$ [30], which is determined to reproduce the exact-Fock energy at the level of the point-particle approximation. Here, $\rho_{\text{ch}}^{p\text{-fin}}$ and $\rho_{\text{ch}}^{pn\text{-fin}}$ are charge densities in which only proton finite size and both proton and neutron finite size are considered, respectively. They are defined in the momentum space as

$$\tilde{\rho}_{\text{ch}}^{p\text{-fin}}(q) = \tilde{G}_{\text{E}p}(q^2)\tilde{\rho}_p(q), \quad (19a)$$

$$\begin{aligned} \tilde{\rho}_{\text{ch}}^{pn\text{-fin}}(q) &= \tilde{G}_{\text{E}p}(q^2)\tilde{\rho}_p(q) + \tilde{G}_{\text{E}n}(q^2)\tilde{\rho}_n(q) \\ &= \tilde{\rho}_{\text{ch}}(q), \end{aligned} \quad (19b)$$

respectively, where $\tilde{\rho}(q)$ is the Fourier transform of the density in the coordinate representation $\rho(r)$. In this paper, we only consider the electric form factors of nucleons, $\tilde{G}_{\text{E}\tau}$ ($\tau = p, n$), and use the form factors obtained by Friedrich and Walcher [67]. We will use ρ_{ch} to calculate the Coulomb energy only: only the electric form factors are considered in Eq. (19) and effects of the magnetic form factors are considered perturbatively as the electromagnetic spin-orbit interaction. Since the vacuum polarization is weak compared to the Coulomb Hartree and exchange terms, the finite-size effect on the vacuum polarization is not considered [29]. On top of "All," the electromagnetic spin-orbit term E_{EMSO} is considered perturbatively, which is abbreviated as "All + EMSO." Since E_{EMSO} is considered at first-order perturbation theory, it does not affect the density distribution, i.e., charge radius or ΔR_{np}.

C. Calculation setup

All the terms shown above have been implemented in the calculation code SKYRME_RPA [68]. The spherical symmetry is assumed and the pairing correlation is neglected in the calculation, since we focus on only the doubly magic nuclei. A meshed box of 0.1 fm × 150 is used.

IV. NUMERICAL RESULTS AND DISCUSSION

This section is devoted to show numerical results: ISB effects on nuclear matter properties and the sensitivity study to the Coulomb interaction and the ISB strength dependence of the following physical observables—the neutron-skin thickness, the difference between the charge radius of ^{40}Ca and that of ^{48}Ca, and mass differences of mirror nuclei of ^{48}Ca - ^{48}Ni isobars. For the first check, we select ^{16}O, ^{40}Ca, ^{48}Ca, ^{48}Ni, and ^{208}Pb as examples to study the neutron-skin thickness.

A. Nuclear matter properties

The parameter sets of SAMi and SAMi-ISB EDFs are optimized by using the same protocol. To see more precise effects of CSB and CIB nuclear matter properties, we switch on and off CSB and CIB terms of SAMi-ISB in Table I. The saturation density ρ_{sat} and EoS parameters ε_{sat}, J, and L defined in Sec. II are calculated by SAMi-noISB, SAMi-CIB, SAMi-CSB, and SAMi-ISB EDFs shown in Table I. To see

TABLE I. The saturation density ρ_{sat} and EoS parameters ε_{sat}, J, and L calculated by SAMi-noISB, SAMi-CIB, SAMi-CSB, and SAMi-ISB EDFs. To see the effect of refitting, those by SAMi EDF are also shown.

EDF		SAMi	SAMi-noISB	SAMi-CIB	SAMi-CSB	SAMi-ISB
E_{IS}		SAMi	SAMi-noISB	SAMi-noISB	SAMi-noISB	SAMi-noISB
E_{CIB}		No	No	Yes	No	Yes
E_{CSB}		No	No	No	Yes	Yes
ρ_{sat}	(fm^{-3})	0.1587	0.1613	0.1597	0.1613	0.1597
$\varepsilon_{\text{sat}} + \varepsilon_{\text{sat}}^{\text{CIB}}$	(MeV)	-15.9271	-16.0288	-15.7700	-16.0288	-15.7700
$J + J^{\text{CIB}} + J^{\text{CSB}}$	(MeV)	28.1256	30.8274	31.4337	29.7667	30.3835
$L + L^{\text{CIB}} + L^{\text{CSB}}$	(MeV)	43.5582	50.0953	52.3624	46.9132	49.2118

the effect of refitting of SAMi and SAMi-noISB, i.e., the effect of difference of Skyrme parameters, t_0–t_3, x_0–x_3, W_0, W_0', and α, results of the original SAMi are also listed. Here, SAMi-noISB, SAMi-CIB, and SAMi-CSB, respectively, refer to SAMi-ISB without any ISB terms, only with CIB term, and only with CSB term. Summary of their abbreviations is also shown in Table I.

The CIB term makes ρ_{sat} smaller and ε_{sat} larger, but their effects are, respectively, less than $0.002\,\text{fm}^{-3}$ and $0.2\,\text{MeV}$, which are negligible. The refitting effect, i.e., difference between ρ_{sat} and ε_{sat} obtained by SAMi and those by SAMi-noISB, is also quite tiny.

The CIB term makes $J + J^{\text{CIB}} + J^{\text{CSB}}$ and $L + L^{\text{CIB}} + L^{\text{CSB}}$ larger, respectively, by $0.6\,\text{MeV}$ and $2.3\,\text{MeV}$ and the CSB term makes them smaller, respectively, by $1.1\,\text{MeV}$ and $3.2\,\text{MeV}$. Effects of these two terms almost cancel each other, and, eventually, $J + J^{\text{CIB}} + J^{\text{CSB}}$ and $L + L^{\text{CIB}} + L^{\text{CSB}}$ obtained by SAMi-noISB and SAMi-ISB are quite similar. In contrast, the refitting effect on J and L are, respectively, $2.7\,\text{MeV}$ and $6.5\,\text{MeV}$. The refitting effect on L may not be negligible.

B. Neutron-skin thickness

1. Coulomb term and L parameter

It has been shown that the neutron-skin thickness ΔR_{np} is related to the density dependence of the symmetry energy of nuclear matter L [39–41,69,70]. First, we show the sensitivity study of the L parameter on the Coulomb part of the EDF. In this calculation, the ISB terms are not considered, i.e., $E_{\text{CSB}} \equiv 0$ and $E_{\text{CIB}} \equiv 0$. For the Coulomb part E_{Coul}, we adopt NoEx, LDA, GGA, p-fin, pn-fin, and All, which are defined in Eqs. (16).

All the calculations are performed with the SAMi EDF and the SAMi-J EDF family. The parameter sets of the SAMi-J family are determined by the same criteria of the SAMi EDF with a fixed symmetry energy J. Accordingly, each SAMi-J EDF has different symmetry parameter L, as shown in Table II. The neutron-skin thickness ΔR_{np} for various L can be calculated using SAMi and SAMi-J EDFs, and the data are fitted to

$$\Delta R_{np} \equiv R_n - R_p = a + bL, \quad (20)$$

i.e., the same as Ref. [40], where R_n and R_p are the root-mean-square radii of the neutron and proton density distributions, respectively.

Panel (a) of Figs. 1–5 shows the neutron-skin thickness ΔR_{np} as a function of the symmetry parameter L for ^{16}O, ^{40}Ca, ^{48}Ca, ^{48}Ni, and ^{208}Pb, respectively. The pentagon, circle, square, up-triangle, down-triangle, and diamond symbols show the results of NoEx, LDA, GGA, p-fin, pn-fin, and All, respectively. Using the data, a and b in Eq. (20) are determined as shown in Table III. Panel (b) of Figs. 1–5 shows the difference between the neutron-skin thickness ΔR_{np} calculated by these Coulomb EDFs and that by the Coulomb LDA EDF. As will be discussed later, the treatment of the Coulomb interaction scarcely affects the neutron-skin thickness ΔR_{np}. The experimental values of ΔR_{np} for ^{40}Ca ($\Delta R_{np} = -0.010^{+0.022}_{-0.023}$ fm [71]), ^{48}Ca ($0.168^{+0.025}_{-0.028}$ fm [71] and 0.121 ± 0.050 fm [72]), and ^{208}Pb ($\Delta R_{np} = 0.211^{+0.054}_{-0.063}$ fm [73], 0.283 ± 0.071 fm [74], and the reanalyzed data of PREX-II experiment $\Delta R_{np} = 0.190 \pm 0.020$ fm [75]) are also shown as vertical lines in Figs. 2, 3, and 5, respectively.

First, let us compare the L dependence of ΔR_{np} among all the calculated nuclei. In $N = Z$ nuclei, the neutron-skin thickness ΔR_{np} is almost independent of the slope parameter L, because b is small $[O(10^{-5})\,\text{MeV}\,\text{fm}^{-1}]$. In contrast, in $N > Z$ nuclei, the neutron-skin thickness ΔR_{np} has a strong L dependence as mentioned in Refs. [40,41] with $b \simeq O(10^{-3})\,\text{MeV}\,\text{fm}^{-1}$. Moreover, as seen in ^{48}Ca and ^{48}Ni, the values b of the mirror nuclei have almost the same absolute value but opposite signs. In contrast, the absolute value a for ^{48}Ni is almost twice of that for ^{48}Ca, which is quite a significant difference considering the isospin symmetry of the

TABLE II. The saturation density ρ_{sat}, the symmetry energy J, and its slope L of the SAMi EDF [59] and the SAMi-J family [60].

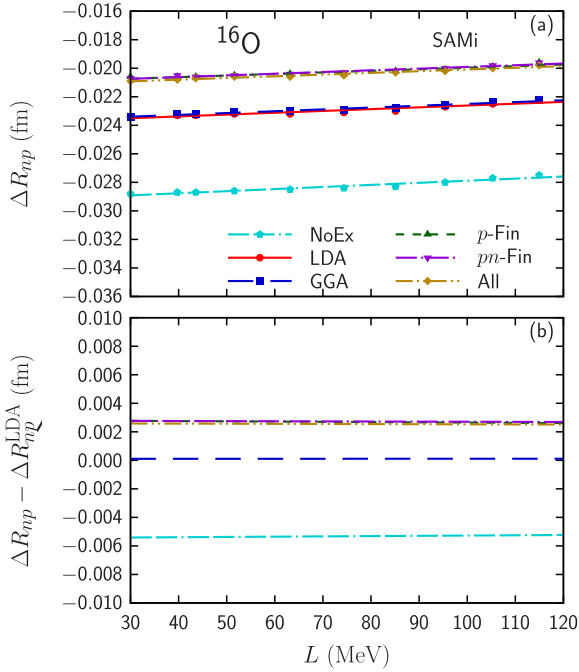| EDF	ρ_{sat} (fm^{-3})	J (MeV)	L (MeV)
SAMi-J27	0.1595	27	30.0001
SAMi-J28	0.1587	28	39.7416
SAMi-J29	0.1579	29	51.6040
SAMi-J30	0.1571	30	63.1784
SAMi-J31	0.1563	31	74.3683
SAMi-J32	0.1555	32	85.1014
SAMi-J33	0.1548	33	95.4072
SAMi-J34	0.1542	34	105.3074
SAMi-J35	0.1537	35	114.9543
SAMi	0.1587	28.1256	43.5582

FIG. 1. (a) Neutron-skin thickness ΔR_{np} as a function of the symmetry parameter L for ^{16}O. The dash-dash-dotted, solid, long-dashed, dashed, dash-dotted, and dash-dot-dotted lines with pentagon, circle, square, up-triangle, down-triangle, and diamond symbols show the results without Coulomb exchange (NoEx), of Coulomb LDA and Coulomb GGA in point-particle approximation (LDA and GGA), of Coulomb GGA with proton and proton-neutron finite-size effects (*p*-fin and *pn*-fin), and of Coulomb GGA with proton-neutron finite-size effects and the vacuum polarization (All), respectively. (b) Change of ΔR_{np} from that of the Coulomb LDA EDF.

nuclear interaction. In these calculations in Figs. 1–5, the ISB terms of the nuclear interaction are not considered, and the effects of the ISB terms of the nuclear interaction are left for the next section. Note that negative values of b in ^{16}O, ^{40}Ca, and ^{48}Ni indicate proton skins, instead of neutron skins. The detailed discussion of the origin of the correlation between ΔR_{np} and L can be found in several papers in the literature, e.g., in Refs. [39,76]. Note that the mean-field calculation sometimes underestimates the isospin impurity [77–79].

Next, we recognize a clear dependence on the treatment of the Coulomb interaction in the value a, i.e., in the absolute value of ΔR_{np}. Even if the treatment of the Coulomb interaction is changed, the L dependence of ΔR_{np} is almost unchanged, i.e., b is almost constant. This is due to the fact that, in the atomic nuclei, the nuclear interaction E_{IS} dominates and the gross structure of ρ_p and ρ_n are determined by E_{IS}. The subdominant Coulomb interaction mainly affects proton distribution, and thus R_p, but its effect on R_p is less than 0.01 fm order. That is, the Coulomb interaction changes the absolute value, and thus a, but it hardly changes the slope b. This is the same as the charge-radii difference of mirror nuclei [37]. The fact that the slope parameter b is hardly changed by the treatment of the Coulomb interaction can be also understood referring to Ref. [80]. Treatment of the
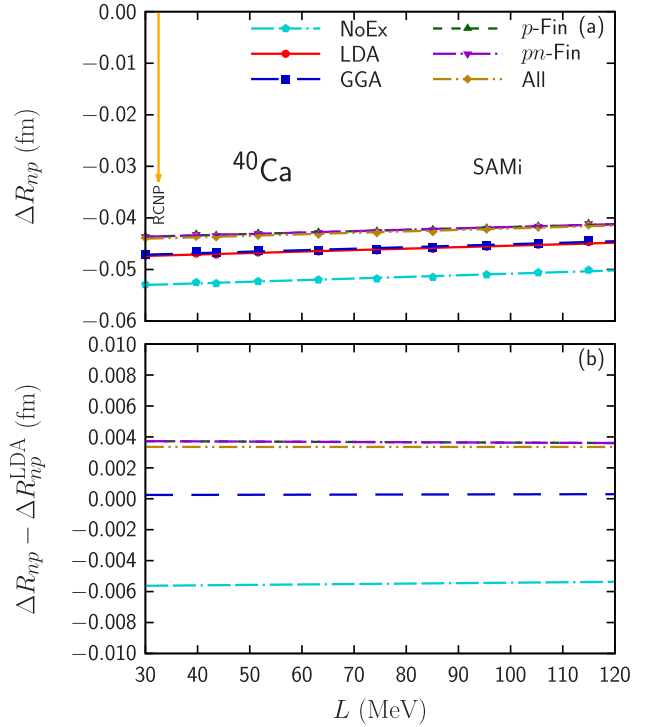

FIG. 2. The same as Fig. 1 but for ^{40}Ca. The experimental value of $\Delta R_{np} = -0.010^{+0.022}_{-0.023}$ fm [71] is shown as a vertical line.
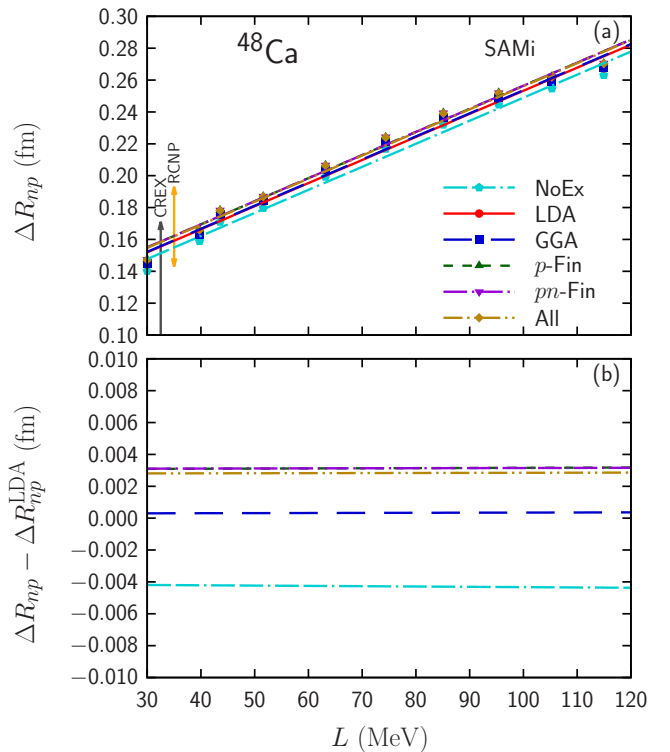

FIG. 3. The same as Fig. 1 but for ^{48}Ca. The experimental value of $\Delta R_{np} = 0.168^{+0.025}_{-0.028}$ fm (RCNP) [71] and 0.121 ± 0.050 fm (CREX) [72] are shown as vertical lines.
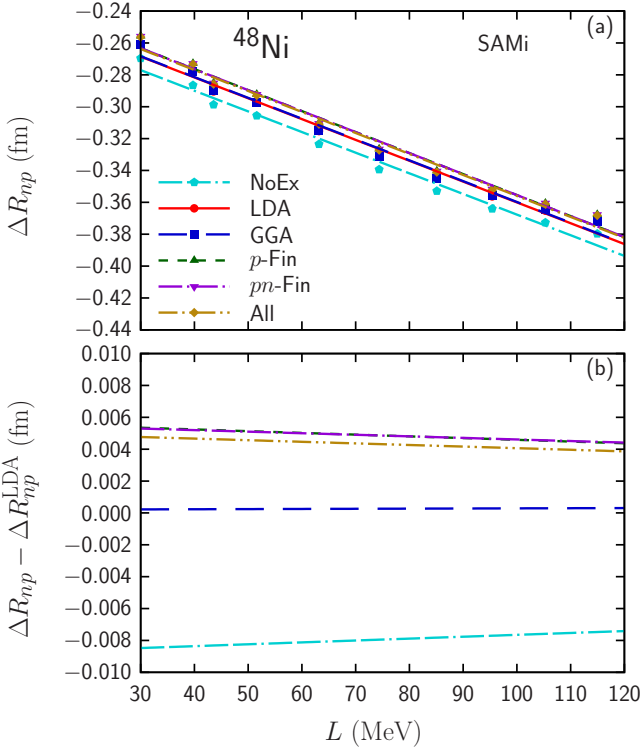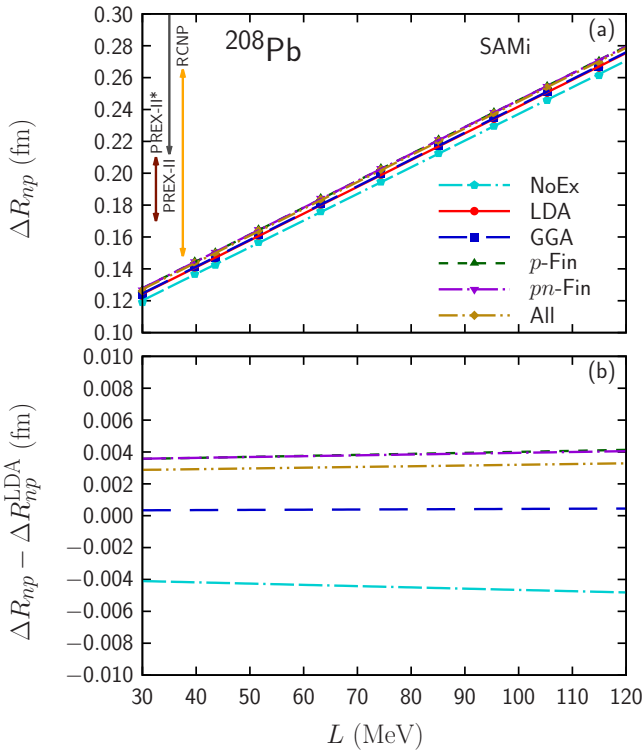
FIG. 4. The same as Fig. 1 but for ^{48}Ni.

FIG. 5. The same as Fig. 1 but for ^{208}Pb. The experimental values of $\Delta R_{np} = 0.211^{+0.054}_{-0.063}$ fm (RCNP) [73] and 0.283 ± 0.071 fm (PREX-II) [74] are shown as vertical lines. Reanalyzed data of PREX-II $\Delta R_{np} = 0.190 \pm 0.020$ fm (PREX-II*) [75] is also shown as a vertical line.

TABLE III. Parameters a and b in Eq. (20). See the text for more detail.

Nuclei	Coulomb	a (fm)	b (fm MeV^{-1})
^{16}O	NoEx	−0.029353	0.00001469
	LDA	−0.023886	0.00001274
	GGA	−0.023782	0.00001283
	p-fin	−0.021061	0.00001097
	pn-fin	−0.021098	0.00001192
	All	−0.021278	0.00001192
^{40}Ca	NoEx	−0.053942	0.00003132
	LDA	−0.048232	0.00002847
	GGA	−0.048001	0.00002903
	p-fin	−0.044467	0.00002712
	pn-fin	−0.044467	0.00002712
	All	−0.044879	0.00002843
^{48}Ca	NoEx	0.104330	0.00144605
	LDA	0.108463	0.00144801
	GGA	0.108747	0.00144866
	p-fin	0.111525	0.00144897
	pn-fin	0.111554	0.00144857
	All	0.111254	0.00144857
^{48}Ni	NoEx	−0.238189	−0.00129505
	LDA	−0.229357	−0.00130689
	GGA	−0.229163	−0.00130595
	p-fin	−0.223682	−0.00131776
	pn-fin	−0.223767	−0.00131670
	All	−0.224293	−0.00131690
^{208}Pb	NoEx	0.069984	0.00167210
	LDA	0.073847	0.00168003
	GGA	0.074152	0.00168124
	p-fin	0.077225	0.00168631
	pn-fin	0.077268	0.00168528
	All	0.076585	0.00168461

Coulomb interaction mainly changes the Coulomb potential in the surface region [30], while the correlation between L and ΔR_{np} of a nucleus with a well-developed bulk like ^{208}Pb is slightly affected by the surface effect [80].

Let us see in more detail the effects of the Coulomb interaction. If the Coulomb exchange term is neglected, ΔR_{np} becomes smaller. Since the Coulomb exchange term E_{Cx} is effectively attractive, the Coulomb effect gets stronger if E_{Cx} is neglected. Then, ρ_p extends, i.e., R_p becomes larger, while ρ_n scarcely changes. As discussed in Ref. [30], the GGA EDF scarcely changes ρ_p nor ρ_n; hence, ΔR_{np} is also scarcely changed. The proton finite-size effect makes the Coulomb interaction between protons weaker [31]. Accordingly, ρ_p shrinks, i.e., R_p becomes smaller, while ρ_n remains almost the same, so that ΔR_{np} becomes larger. In contrast, the vacuum polarization makes the Coulomb interaction between protons stronger and thus ΔR_{np} becomes smaller.

To understand the effect of neutron finite size to ΔR_{np}, we introduce here the effective charge formalism to implement the finite-size effect. For simplicity, we consider only the Hartree term, while it can be straightforwardly extended to the Coulomb exchange term. If the effective charges of the protons and neutrons, $e_{\mathrm{eff}\,p}$ and $e_{\mathrm{eff}\,n}$, are
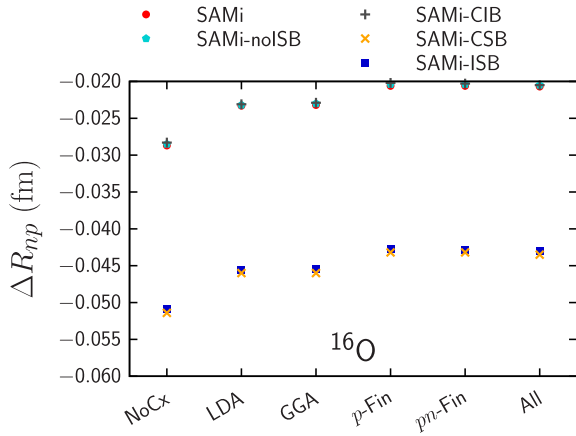
FIG. 6. Neutron-skin thickness of ^{16}O calculated with several Coulomb treatment with SAMi (circle), SAMi-noISB (pentagon), SAMi-CIB (plus), SAMi-CSB (cross), and SAMi-ISB (square) EDFs.

introduced,[2] the charge density distributions are written as

$$\rho_{\text{ch}}(\boldsymbol{r}) \simeq e_{\text{eff}p}\rho_p(\boldsymbol{r}) + e_{\text{eff}n}\rho_n(\boldsymbol{r}). \tag{21}$$

Here, $e_{\text{eff}n}$ is assumed to be negative since the mean-square radius of neutron charge distribution $r_{\text{E}n}^2$ is negative. Since $e_{\text{eff}n}$ is negative, the proton-neutron Coulomb interaction is attractive. At the same time, ρ_{ch} shrinks when the neutron finite-size effect is considered, because of $e_{\text{eff}n} < 0$. Therefore, the behavior is rather complicated, and eventually, the intercept a is almost unchanged, because the neutron finite-size effect is weak.

At last, we discuss how much the Coulomb interaction affects the estimation of L value from ΔR_{np} in ^{208}Pb. Here, uncertainties due to the linear fitting is not considered. For instance, if $\Delta R_{np} = 0.20$ fm is assumed, adopting the present estimations with the Coulomb LDA EDF, the slope parameter

---

[2]The effective charges may have $\boldsymbol{r}$, Z, or N dependences, while such dependences are not considered here for simplicity.
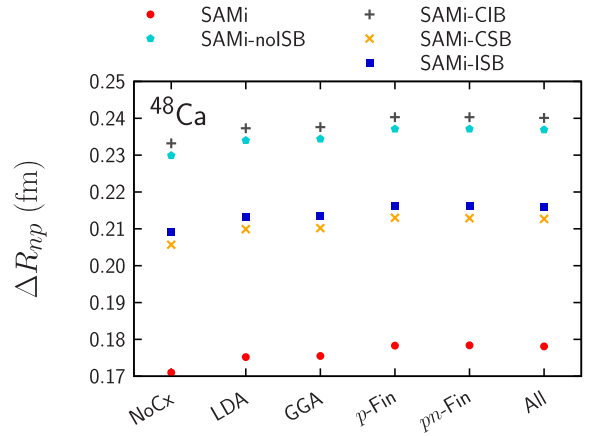

FIG. 8. The same as Fig. 6 but for ^{48}Ca.

is estimated as $L = 75$ MeV, while it is estimated as 73 MeV with the All Coulomb EDF. This difference is much smaller than the experimental error or uncertainty due to the linear fitting. The treatment of the Coulomb interaction does not impact much on the extraction of L from the experimental result for ΔR_{np}.

2. Comparison between Coulomb and ISB interactions

Next, we show the dependence of the treatment of the Coulomb interaction and the ISB interaction on ΔR_{np} in Figs. 6–10. Circles, pentagons, pluses, crosses, and squares show calculated results with SAMi, SAMi-noISB, SAMi-CIB, SAMi-CSB, and SAMi-ISB EDFs, respectively. Their values in ^{40}Ca, ^{48}Ca, and ^{208}Pb are also shown in Table IV.

Both the CSB and CIB terms contribute to ΔR_{np}: The former decreases ΔR_{np} for both $N = Z$ and $N \neq Z$ nuclei; the latter slightly decreases ΔR_{np} in $N < Z$ nuclei, whereas it slightly increases for $N > Z$ nuclei. The CIB term does not affect ΔR_{np} in $N = Z$ nuclei. The values of the CSB and CIB contributions can be found in Table IV and Figs. 6–10.

It is shown that SAMi and SAMi-noISB give almost the same ΔR_{np} in $N = Z$ nuclei, while SAMi-noISB gives larger (smaller) ΔR_{np} than SAMi in $N > Z$ ($N < Z$) nuclei. In
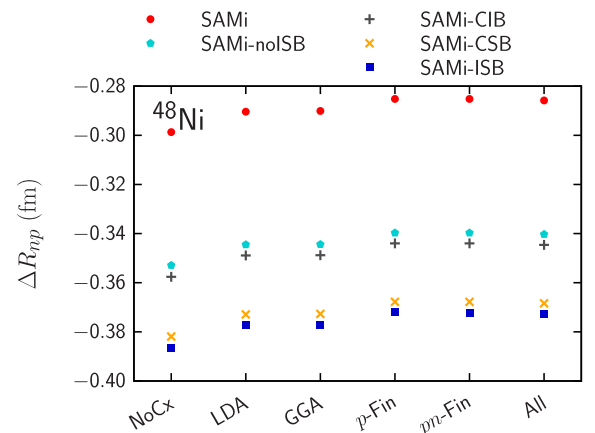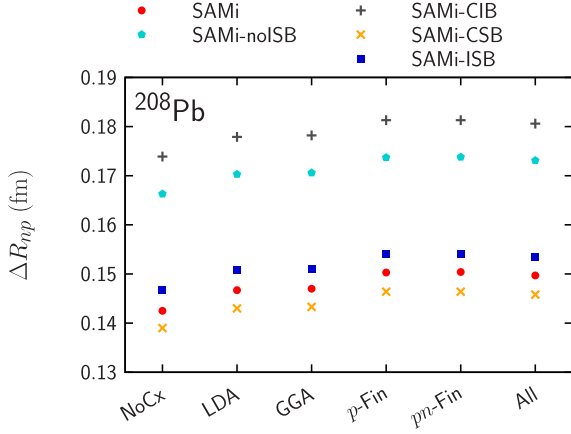

FIG. 7. The same as Fig. 6 but for ^{40}Ca.

FIG. 9. The same as Fig. 6 but for ^{48}Ni.

FIG. 10. The same as Fig. 6 but for ^{208}Pb.

FIG. 11. Neutron-skin thickness ΔR_{np} as functions of the CSB and CIB strength $-s_0$ and u_0, respectively, for ^{16}O. The long-dashed and dashed lines show results only with CSB and only with CIB, respectively. Filled and empty arrows show ΔR_{np} calculated by the full SAMi-ISB and the SAMi EDFs, respectively.

$N = Z$ nuclei, if neither the ISB interaction nor the Coulomb interaction is considered, ΔR_{np} is equal to zero due to the isospin symmetry. Thus, ΔR_{np} of the SAMi and SAMi-noISB are constructed only due to the Coulomb interaction, and thus these two EDFs give the similar ΔR_{np} in $N = Z$ nuclei. In contrast, $N \neq Z$ nuclei, difference between the SAMi and the SAMi-noISB reflects the property of these EDFs, especially their L values (SAMi: $L = 44$ MeV, SAMi-noISB: $L = 50$ MeV).

Comparing how ΔR_{np} is changed as the Coulomb interaction is treated precisely step-by-step, one can find that such changes are universal among the results calculated with the SAMi, SAMi-noISB, SAMi-CIB, SAMi-CSB, and SAMi-ISB. Thus, one can conclude that the effect of the model dependence associated with the treatment of the Coulomb interaction is unchanged [$O(0.001)$ fm], which is comparable with the effect of the CIB term on ΔR_{np} for $N \neq Z$ nuclei.

References [8,9,81] claimed that the ISB interaction and the Coulomb exchange give a nontrivial cancellation. If the claim in Refs. [8,9,81] is valid, ΔR_{np} calculated with the SAMi EDF without the Coulomb exchange term and that with the SAMi-ISB EDF with the Coulomb LDA exchange (or all the Coulomb) term should be identical. However, as seen in Table IV and Figs. 6–10, ΔR_{np} for ^{40}Ca, ^{48}Ca, and ^{208}Pb calculated with the SAMi without the Coulomb exchange term are -0.0527, 0.1710, and 0.1425 fm, respectively, whereas those with the SAMi-ISB and the Coulomb exchange (all Coulomb) are -0.0706, 0.2133, and 0.1508 fm (-0.0672,
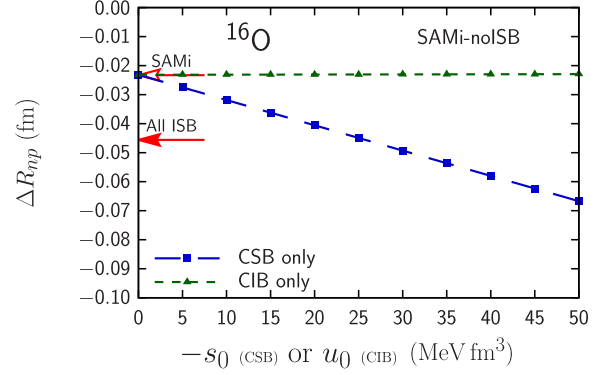
0.2160, and 0.1534 fm); these two are still non-negligibly different, except ^{208}Pb. The case of ^{208}Pb may be accidental. Thus, such treatment is not fully acceptable to discuss ΔR_{np} quantitatively.

3. ISB term and neutron-skin thickness

At last, we study how much the ISB strength correlates with the neutron-skin thickness ΔR_{np}. In this calculation, the SAMi-noISB EDF is used for E_{IS}. The CSB strength $-s_0$ in E_{CSB} is gradually changed from 0 MeV fm^3 to 50 MeV fm^3, while the CIB strength u_0 in E_{CIB} is kept 0 MeV fm^3, or the CIB strength u_0 in E_{CIB} is gradually changed from 0 MeV fm^3 to 50 MeV fm^3, while $E_{CSB} = 0$ MeV fm^3 is kept. Note that this calculation with $u_0 = 25.8$ MeV fm^3 and $-s_0 = 26.3$ MeV fm^3 exactly corresponds to the SAMi-ISB EDF. The Coulomb LDA EDF [Eq. (16b)] is used for the calculation.

Using these data, u_0 or $-s_0$ dependence of ΔR_{np} is parametrized as

$$\Delta R_{np} = c + d(-s_0), \tag{22a}$$

$$\Delta R_{np} = e + f u_0. \tag{22b}$$

Figures 11–15 show the neutron-skin thickness ΔR_{np} as functions of the ISB strength $-s_0$ and u_0 for ^{16}O, ^{40}Ca, ^{48}Ca, ^{48}Ni, and ^{208}Pb. Since the refitting effect of the Skyrme EDF is non-negligible, the experimental data are not shown in the

TABLE IV. Neutron-skin thickness ΔR_{np} of ^{40}Ca, ^{48}Ca, and ^{208}Pb calculated with SAMi-ISB EDF without Coulomb exchange term (NoCx), with Coulomb LDA (LDA), or with full Coulomb treatment (All) without ISB term, only with CSB term, only with CIB term, and with all ISB terms. For comparison, ΔR_{np} calculated with the SAMi EDF is also shown. All the values are in fm.

E_{IS}	ISB	^{40}Ca			^{48}Ca			^{208}Pb		
		NoCx	LDA	All	NoCx	LDA	All	NoCx	LDA	All
SAMi	No ISB	-0.0527	-0.0471	-0.0437	0.1710	0.1752	0.1781	0.1425	0.1467	0.1497
SAMi-noISB	No ISB	-0.0514	-0.0460	-0.0426	0.2299	0.2340	0.2369	0.1663	0.1703	0.1731
SAMi-noISB	Only CIB	-0.0512	-0.0458	-0.0424	0.2332	0.2373	0.2401	0.1739	0.1779	0.1806
SAMi-noISB	Only CSB	-0.0767	-0.0712	-0.0678	0.2057	0.2099	0.2127	0.1390	0.1430	0.1458
SAMi-noISB	All ISB	-0.0760	-0.0706	-0.0672	0.2092	0.2133	0.2160	0.1468	0.1508	0.1534
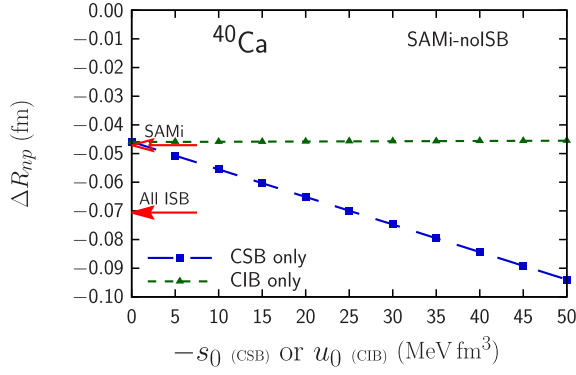
FIG. 12. The same as Fig. 11 but for ^{40}Ca.

FIG. 14. The same as Fig. 11 but for ^{48}Ni.

figures. The long-dashed and dashed lines show the results only with CSB and only with CIB, respectively. Filled and empty arrows show ΔR_{np} calculated by the full SAMi-ISB and the original SAMi EDFs, respectively. Using the data, c and d in Eq. (22a) and e and f in Eq. (22b) are determined as shown in Table V.
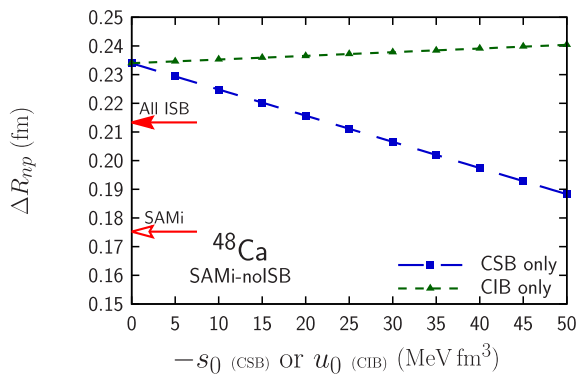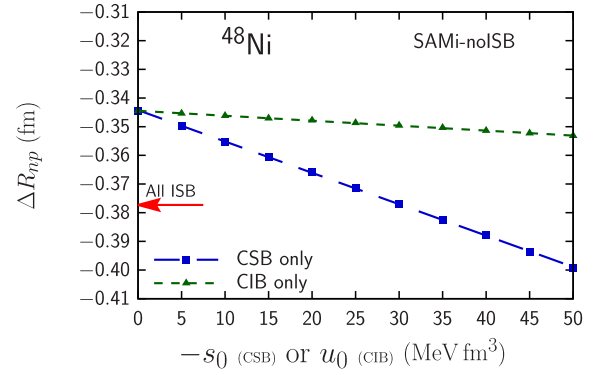
The CSB strength makes ΔR_{np} smaller and its slope d has almost the same value, $d \simeq -0.001\,\text{MeV}^{-1}\,\text{fm}^{-2}$, among all the calculated nuclei. On the other hand, a larger CIB strength changes ΔR_{np} around 10–20% of the CSB case in $N \neq Z$ nuclei, while around 0.5–1% in $N = Z$ nuclei. Moreover, ΔR_{np} becomes larger in $N > Z$ nuclei and smaller in $N < Z$ nuclei as the CIB strength u_0 becomes larger. The absolute value of the change of ΔR_{np} is almost the same among the mirror nuclei. Eventually, the CSB term gives the dominant contribution to ΔR_{np}, and the ISB contribution to ΔR_{np} is qualitatively universal in all the selected nuclei.

We will consider the main reason of such behaviors.[3] The Skyrme-like zero-range CSB interaction for proton-proton, proton-neutron, and neutron-neutron are [7,22]

$$v_{\text{CSB}}^{pp}(\mathbf{r}_1, \mathbf{r}_2) = -\frac{s_0}{2}(1 - P_\sigma)\delta(\mathbf{r}_1 - \mathbf{r}_2), \qquad (23a)$$

$$v_{\text{CSB}}^{pn}(\mathbf{r}_1, \mathbf{r}_2) = 0, \qquad (23b)$$

_____

[3]The mechanism how the CSB interaction affects ΔR_{np} was already discussed in the previous paper [36].

$$v_{\text{CSB}}^{nn}(\mathbf{r}_1, \mathbf{r}_2) = +\frac{s_0}{2}(1 - P_\sigma)\delta(\mathbf{r}_1 - \mathbf{r}_2), \qquad (23c)$$

respectively, with $s_0 < 0$. Hence, as $|s_0|$ becomes larger, the proton-proton repulsive interaction and the neutron-neutron attractive interaction become stronger. Accordingly, ρ_p expands and ρ_n shrinks. Consequently, ΔR_{np} becomes smaller as $|s_0|$ becomes larger.

On the contrary, the Skyrme-like zero-range CIB interaction for proton-proton, proton-neutron, and neutron-neutron are [7,22]

$$v_{\text{CIB}}^{pp}(\mathbf{r}_1, \mathbf{r}_2) = +\frac{u_0}{2}(1 - P_\sigma)\delta(\mathbf{r}_1 - \mathbf{r}_2), \qquad (24a)$$

$$v_{\text{CIB}}^{pn}(\mathbf{r}_1, \mathbf{r}_2) = -\frac{u_0}{2}(1 - P_\sigma)\delta(\mathbf{r}_1 - \mathbf{r}_2), \qquad (24b)$$

$$v_{\text{CIB}}^{nn}(\mathbf{r}_1, \mathbf{r}_2) = +\frac{u_0}{2}(1 - P_\sigma)\delta(\mathbf{r}_1 - \mathbf{r}_2), \qquad (24c)$$

respectively, with $u_0 > 0$. Hence, as u_0 becomes larger, the proton-proton and neutron-neutron repulsive interactions and the proton-neutron attractive interaction become stronger. The effective CIB potential for protons and neutrons read

$$
\begin{aligned}
V_{\text{CIB}}^p(\mathbf{r}) &= \frac{\delta E_{\text{CIB}}[\rho_p, \rho_n]}{\delta \rho_p(\mathbf{r})} \\
&= \frac{u_0}{2}\rho_p(\mathbf{r}) - \frac{u_0}{4}\rho_n(\mathbf{r}) \\
&= \frac{u_0}{4}[2\rho_p(\mathbf{r}) - \rho_n(\mathbf{r})], \qquad (25a)
\end{aligned}
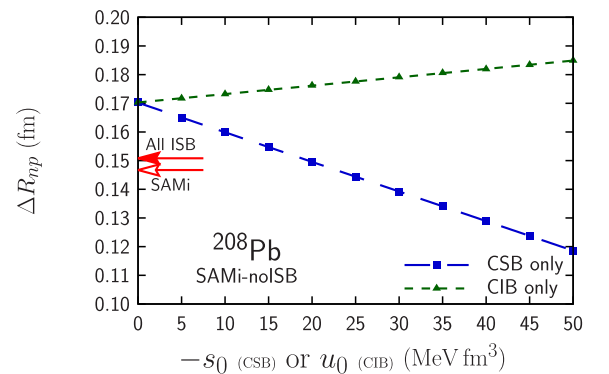$$

FIG. 13. The same as Fig. 11 but for ^{48}Ca.

FIG. 15. The same as Fig. 11 but for ^{208}Pb.

TABLE V. Parameters c, d, e, and f in Eqs. (22). See text for more detail.

Nuclei	ISB	c or e (fm)	d or f (MeV^{-1} fm^{-2})
^{16}O	CSB	-0.023145	-0.00087127
	CIB	-0.023168	0.00000455
^{40}Ca	CSB	-0.045923	-0.00096055
	CIB	-0.045986	0.00000927
^{48}Ca	CSB	0.233945	-0.00091309
	CIB	0.233977	0.00012818
^{48}Ni	CSB	-0.344227	-0.00109382
	CIB	-0.344459	-0.00017291
^{208}Pb	CSB	0.170209	-0.00103236
	CIB	0.170300	0.00029200

$$
\begin{aligned}
V_{\mathrm{CIB}}^{n}(\boldsymbol{r}) &= \frac{\delta E_{\mathrm{CIB}}[\rho_p, \rho_n]}{\delta \rho_n(\boldsymbol{r})} \\
&= \frac{u_0}{2}\rho_n(\boldsymbol{r}) - \frac{u_0}{4}\rho_p(\boldsymbol{r}) \\
&= \frac{u_0}{4}[2\rho_n(\boldsymbol{r}) - \rho_p(\boldsymbol{r})], \quad (25\mathrm{b})
\end{aligned}
$$

respectively. In $N = Z$ nuclei, the proton and neutron density distributions are approximately the same, $\rho_p(\boldsymbol{r}) \simeq \rho_n(\boldsymbol{r})$.

$$
\Delta R_{np} = \begin{cases}
0.001680(L + L^{\mathrm{CIB}} + L^{\mathrm{CSB}}) + 0.07385 & \text{(without ISB terms)}, \\
0.001661(L + L^{\mathrm{CIB}} + L^{\mathrm{CSB}}) + 0.07907 & \text{(only with CIB term)}, \\
0.001698(L + L^{\mathrm{CIB}} + L^{\mathrm{CSB}}) + 0.04987 & \text{(only with CSB term)}, \\
0.001678(L + L^{\mathrm{CIB}} + L^{\mathrm{CSB}}) + 0.05526 & \text{(with all ISB terms)},
\end{cases} \quad (26)
$$

and are shown in Fig. 16. If the same ΔR_{np} is assumed, the difference between obtained $L + L^{\mathrm{CIB}} + L^{\mathrm{CSB}}$ without any ISB
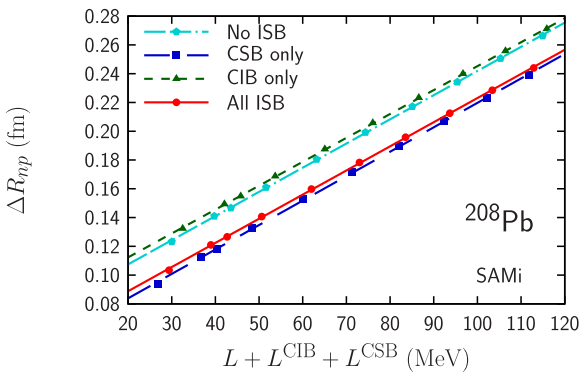

FIG. 16. Correlation between $L + L^{\mathrm{CIB}} + L^{\mathrm{CSB}}$ and ΔR_{np} calculated without any ISB terms, only with CSB term, only with CIB term, and with the all ISB terms, respectively, shown in dash-dotted, long-dashed, dashed, and solid lines. The ISB terms of the SAMi-ISB EDF [Eqs. (14) and (15)] are considered on top of the SAMi EDF and SAMi-J family.

Therefore, $V_{\mathrm{CIB}}^{p}(\boldsymbol{r}) \simeq V_{\mathrm{CIB}}^{n}(\boldsymbol{r})$ also holds, and thus the CIB effect on R_p is almost same as that on R_n. Hence, even though R_p and R_n are changed as the CIB strength u_0 is changed, the neutron-skin thickness ΔR_{np} is almost unchanged. In $N > Z$ nuclei, in general, $\rho_n(\boldsymbol{r}) > \rho_p(\boldsymbol{r})$ holds, and thus the repulsive potential V_{CIB}^{p} is weaker than V_{CIB}^{n}, i.e., $V_{\mathrm{CIB}}^{p} < V_{\mathrm{CIB}}^{n}$. Hence, R_n extends more than R_p, and accordingly, ΔR_{np} increases. Since V_{CIB}^{p} is approximately equal to V_{CIB}^{n} of the mirror nucleus, the behaviors among the mirror nuclei have the same magnitude but with opposite signs.

At last, we will discuss how large the CSB and CIB strengths affect the estimation of L value. Here, ^{208}Pb is taken as an example. As we did in Sec. IV B 1 and Ref. [37], the L-ΔR_{np} correlation is derived by using the SAMi EDF and SAMi-J family. Because the pressure of neutron matter is proportional to $L + L^{\mathrm{CIB}} + L^{\mathrm{CSB}}$, the neutron-skin thickness is also expected to be correlated with $L + L^{\mathrm{CIB}} + L^{\mathrm{CSB}}$. If one does not consider CIB or CSB term, L^{CIB} and L^{CSB} are equal to zero.

In order to see the ISB contribution, the ISB terms of the SAMi-ISB EDF [Eqs. (14) and (15)] are considered on top of the SAMi EDF and SAMi-J family. The correlations without any ISB terms, only with CIB term, only with CSB term, and with both the CSB and CIB terms, denoted by all ISB, respectively, read

terms and that with all ISB terms is 11.1 MeV. Using $L^{\mathrm{CIB}} = 2.3$ MeV and $L^{\mathrm{CSB}} = -3.2$ MeV, one finds that L itself is changed by 12.0 MeV once the ISB terms are considered. Thus, the ISB contributions, in particular, the CSB one, to the L parameter may not be negligible. In contrast to the case of the charge-radii difference of mirror nuclei ΔR_{ch}, the effect on L is smaller. This is because the CIB effect and the CSB one is opposite direction in ΔR_{np} for $N > Z$ nuclei, while they are coherent in ΔR_{ch}. It should be noted that once E_{IS} is refitted with considering the ISB terms, the effect of ISB terms becomes rather mild. Here, the uncertainty due to the fitting is not considered, since both correlations between L and ΔR_{np} and that between ISB strengths and ΔR_{np} obtained in this paper are almost perfect (with $r \approx 1.000$), and accordingly, the uncertainty due to the correlation is negligible.

C. Charge radii difference between ^{40}Ca and ^{48}Ca

Figure 17 shows the CSB- and CIB-strength, $-s_0$ and u_0, dependences of the difference of charge radii, $R_{\mathrm{ch}}^{\text{Ca-48}} - R_{\mathrm{ch}}^{\text{Ca-40}}$. Here, the root-mean-square radius R_{ch} is calculated by

$$
R_{\mathrm{ch}}^2 = \int r^2 \rho_{\mathrm{ch}}(\boldsymbol{r})\,d\boldsymbol{r} + R_{\mathrm{so}}^2, \quad (27)
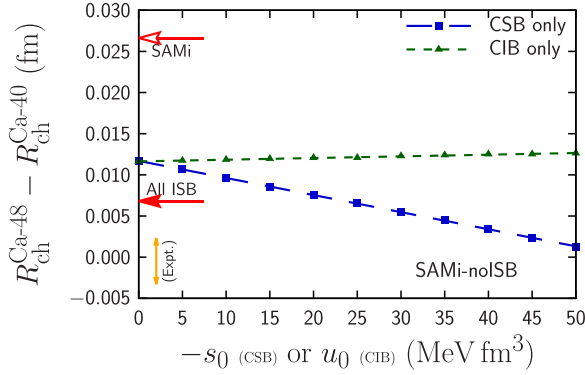$$

FIG. 17. The CSB and CIB strength, $-s_0$ and u_0, dependences of the difference of the calculated charge radius of ^{40}Ca and that of ^{48}Ca. Experimental value taken from Ref. [85] is shown as a vertical line.
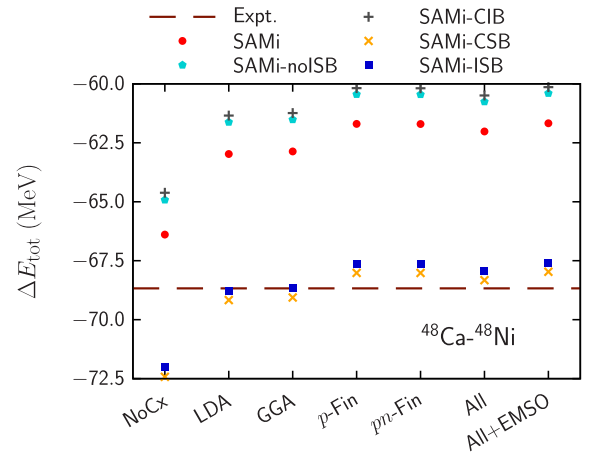

FIG. 18. The mass difference of mirror nuclei ^{48}Ca - ^{48}Ni calculated with several Coulomb treatment with SAMi (circle), SAMi-noISB (pentagon), SAMi-CIB (plus), SAMi-CSB (cross), and SAMi-ISB (square) EDFs. Experimental data is taken from AME2020 [86].

where ρ_{ch} is the charge density distribution calculated by using Eq. (19), which only includes effects of nucleon electric form factors, and R_{so}^2 is the spin-orbit (magnetic) contribution to charge radius [82–84]. The spin-orbit contribution can be calculated as $R_{\mathrm{so}}^2 = 0\,\mathrm{fm}^2$ and $-0.101\,\mathrm{fm}^2$ for ^{40}Ca and ^{48}Ca, respectively. As we did in Sec. IV B 3, on top of the SAMi-noISB EDF, the CSB or CIB strength, $-s_0$ or u_0, is gradually changed from $0\,\mathrm{MeV\,fm}^3$ to $50\,\mathrm{MeV\,fm}^3$. These data are fitted to

$$R_{\mathrm{ch}}^{\mathrm{Ca\text{-}48}} - R_{\mathrm{ch}}^{\mathrm{Ca\text{-}40}} = 0.011697 - 2.0767 \times 10^{-4}(-s_0), \tag{28a}$$

$$R_{\mathrm{ch}}^{\mathrm{Ca\text{-}48}} - R_{\mathrm{ch}}^{\mathrm{Ca\text{-}40}} = 0.011637 + 2.0297 \times 10^{-5}u_0, \tag{28b}$$

respectively.

Since the proton numbers of both nuclei are the same ($Z = 20$), the difference of the proton radii, and thus the charge radii, is due to the proton-neutron interaction. As shown in Eqs. (23) and (24), the attractive CIB interaction exists between protons and neutrons, but the CSB interaction does not. Thus, one may think that the CIB strength u_0 influences the difference more than the CSB one. Nonetheless, the figure shows a puzzling behavior; the CSB strength affects the difference, while the CIB strength scarcely does.

To understand such a behavior, let us consider the nuclear EoS. As shown in Sec. II, the CSB and CIB interactions, respectively, give β and β^2 dependences on nuclear EoS [see Eq. (6)]. In the case of ^{48}Ca, the isospin asymmetry is approximately $\beta \approx (28 - 20)/48 = 0.17$. Because ε_1 is negative, whereas $\varepsilon_2^{\mathrm{IS}} \simeq J$ and $3u_0\rho/16$ are positive, the slope of the CIB dependence is opposite to that of the CSB dependence. Since $0 < \beta < 1$ and $|\varepsilon_1|$ is almost the same value of the CIB contribution to $\varepsilon_2^{\mathrm{CIB}}$, the CSB contribution, which is the leading order with respect to β, gives larger contribution. It should also be noted that different models of the Coulomb interaction give almost the same $R_{\mathrm{ch}}^{\mathrm{Ca\text{-}48}} - R_{\mathrm{ch}}^{\mathrm{Ca\text{-}40}}$, since both nuclei have the same proton numbers.

D. Mass difference of mirror nuclei

In this section, we discuss the model dependence of the mass difference of mirror nuclei. The ^{48}Ca - ^{48}Ni pair is selected as an example, $\Delta E_{\mathrm{tot}} = E_{\mathrm{tot}}^{\mathrm{Ca\text{-}48}} - E_{\mathrm{tot}}^{\mathrm{Ni\text{-}48}}$.

First, the dependence on the treatment of Coulomb interaction is shown in Fig. 18. The difference of two estimated binding energies (416.00120 MeV for ^{48}Ca and 347.3 MeV for ^{48}Ni) taken from AME2020 [86] is shown as a horizontal line.[4]

As discussed in Ref. [31], the SAMi-ISB EDF reproduces the experimental value given by the AME2020. The model dependence of Coulomb energy is about 1.2 MeV and does not change this conclusion much. Next, we focus on the comparison between the ISB and Coulomb effects. First, effect of the precise treatment of Coulomb interaction is almost the same among all the tested E_{nucl}. Comparing results by SAMi-noISB and SAMi-ISB, the ISB effects to ΔE_{tot} are around 7.2 MeV. This is basically the effect of the CSB term, whereas the effect of the CIB term on less than 0.3 MeV. The difference between ΔE_{tot} calculated by using SAMi and that by using SAMi-ISB is around 5.8 MeV.

Moreover, although the effects of the exchange term (or more precise treatment) of the Coulomb interaction are partially canceled with that of the ISB terms, the difference between ΔE_{tot} calculated with the SAMi EDF without Coulomb exchange term and that with the SAMi-ISB EDF with the Coulomb exchange (or all the Coulomb) term is still non-negligibly different. Thus, the nontrivial cancellation claimed in Refs. [8,9,81] is not perfect.

We discuss the effects of the CSB and CIB strength on ΔE_{tot}. As we did in Sec. IV B 3, on top of the SAMi-noISB EDF, the CSB or CIB strength, $-s_0$ or u_0, is gradually changed from $0\,\mathrm{MeV\,fm}^3$ to $50\,\mathrm{MeV\,fm}^3$. The CSB- or CIB-strength

---

[4]The binding energy of ^{48}Ni has not been measured yet, and this value is estimated value.
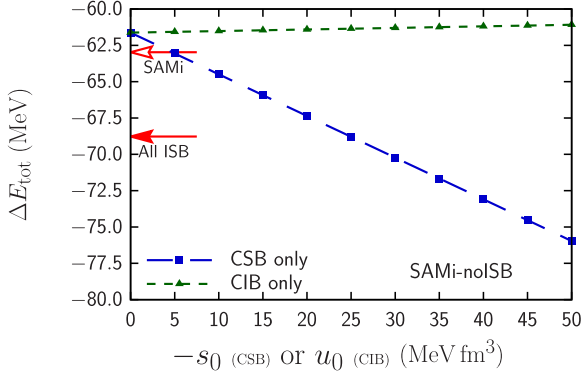
FIG. 19. The mass difference of mirror nuclei ^{48}Ca - ^{48}Ni as functions of CSB (square) and CIB (up-triangle) strength $-s_0$ and u_0. Filled and empty arrows show ΔR_{np} calculated by the full SAMi-ISB and the SAMi EDFs, respectively.

dependence of $\Delta E_{\rm tot}$ is shown in Fig. 19 in the squares and up-triangles, respectively. These data are fitted to

$$\Delta E_{\rm tot} = -61.625 - 0.28677(-s_0), \tag{29a}$$
$$\Delta E_{\rm tot} = -61.625 + 0.01083 u_0, \tag{29b}$$

respectively. As seen in the figure, the mass difference of mirror nuclei $\Delta E_{\rm tot}$ is sensitive to the CSB strength s_0. In contrast, it is not sensitive to the CIB strength u_0, although the absolute value of the total energy is changed. This mechanism is discussed in details in Ref. [36].

V. CONCLUSION

In the previous Letter [37], we had discussed the effects of the Coulomb and the isospin symmetry breaking (ISB) terms of nuclear interactions on the charge-radii difference of mirror nuclei pair ^{48}Ca and ^{48}Ni, $\Delta R_{\rm ch}$. We had found that the ISB terms of the nuclear interaction affect the estimation of the density dependence of the symmetry energy, $L + L_{\rm CSB} + L_{\rm CIB}$, by about 6–14 MeV, using the correlation with $\Delta R_{\rm ch}$. In this paper, we performed similar analyses, i.e., the sensitivity checks of the model dependence of the Coulomb energy and the ISB nuclear interaction to other properties related to the isospin symmetry breaking: the neutron-skin thickness ΔR_{np} of several doubly magic nuclei, the difference of the charge radii between ^{40}Ca and ^{48}Ca, and the mass difference of mirror nuclei between ^{48}Ca and ^{48}Ni.

It is found that even if we treat the Coulomb interaction precisely, its effect on ΔR_{np} is less than 0.01 fm in respect to L. This difference does not affect the extraction of L from the experimental ΔR_{np}.

The ISB terms of the nuclear interaction is divided into two parts: the charge-symmetry breaking (CSB) and the charge-independence breaking (CIB) ones. The CSB interaction has a clear manifestation in the neutron-skin thickness and the mass differences of mirror nuclei. In contrast, the CIB interaction does not have a significant effect on either the neutron-skin thickness of $N = Z$ nuclei or the mass difference of mirror nuclei. The neutron-skin thickness of $N \neq Z$ nuclei is affected by the CIB strength, while its effect is small compared to the CSB and the Coulomb interaction in some cases. Therefore,

if one attempts to discuss effects of the CIB interaction on nuclear properties, the Coulomb interaction must be treated precisely as well.

The difference of the calculated charge radii of ^{40}Ca and ^{48}Ca is claimed to be related to the symmetry energy [38,87]. In this paper, it was confirmed that the strength of the CSB interaction is correlated to such difference as well, while the CIB one does not much. Among all the physical observables we tested, effects of the CIB interaction are smaller than those of the CSB one, or even invisible on all the observables we discussed.

Since both the CSB and the CIB interactions affect ΔR_{np} appreciably, the estimation of $L + L_{\rm CSB} + L_{\rm CIB}$ is also affected because of the strong correlation between two quantities. For instance, if one assumes the CSB and CIB strengths as those used in the SAMi-ISB, their effect to L estimated from the correlation with ΔR_{np} is 12 MeV. Therefore, in order to estimate L parameter using such experimental observables, ISB contribution should be considered, which has not been considered in the previous estimations of L [88,89]. Note that the CSB effect on ΔR_{np} is opposite to the CIB one, whereas they are coherent in $\Delta R_{\rm ch}$. Hence, the net ISB effect on ΔR_{np} is slightly smaller than that on $\Delta R_{\rm ch}$.

It was claimed that the Coulomb exchange term and the ISB of the nuclear interaction are canceled each other, and accordingly the fitting of EDF without the Coulomb exchange term was performed, in some Skyrme EDF, such as the SKX EDF [8,9]. However, we found that such treatment leads to non-negligible error for both ΔR_{np} and $\Delta E_{\rm tot}$ in comparison with proper inclusion of both the Coulomb exchange and ISB interactions.

The magnitude of the ISB effect discussed above obviously depends on the strengths of CSB and CIB interactions. Although the ISB terms affect most nuclear properties, they should be taken into account properly, especially, for several nuclear properties, for instance, ΔR_{np}, $\Delta E_{\rm tot}$, and ΔR_{np}. Thus, it is important to pin down their strengths precisely. We had discussed the possibility of determining the CSB strength in comparison with the physical observables before [36], while we found that phenomenological estimation of the CSB strength based on density functional theory is 5–10 times larger than the *ab initio* estimation in the previous Letter [37]. In this paper, we found that the CIB interaction is insensitive to ΔR_{np}, $\Delta E_{\rm tot}$, and $\Delta R_{\rm ch}$. Hence, it is also important to find measurable quantities sensitive to the CIB strength.

APPENDIX A: ISOSPIN DEPENDENCE OF CIB INTERACTION EXTRACTED FROM ONE-PION EXCHANGE INTERACTION

In this Appendix, the isospin dependence of CIB interaction is discussed. The main origin of the CIB interaction is mass difference of the neutral pion π^0 and charged one $\pi^\pm$. Here, m_{π^0} and $m_{\pi^\pm}$ denote mass of π^0 and $\pi^\pm$, respectively. The one-pion exchange potential reads [90,91]

$$V_{\mathrm{OPEP}}(m_\pi, \boldsymbol{q}) \sim -\frac{(\boldsymbol{\sigma}_1 \cdot \boldsymbol{q})(\boldsymbol{\sigma}_2 \cdot \boldsymbol{q})}{m_\pi^2 + q^2} \boldsymbol{\tau}_1 \cdot \boldsymbol{\tau}_2. \tag{A1}$$

Once the mass difference $m_{\pi^0} \neq m_{\pi^\pm}$ is considered,

$$
\begin{aligned}
V_{\mathrm{OPEP}}(m_{\pi^0}, \boldsymbol{q}) - V_{\mathrm{OPEP}}(m_{\pi^\pm}, \boldsymbol{q}) &\sim -\frac{(\boldsymbol{\sigma}_1 \cdot \boldsymbol{q})(\boldsymbol{\sigma}_2 \cdot \boldsymbol{q})}{m_{\pi^0}^2 + q^2} \tau_{z1} \tau_{z2} + \frac{(\boldsymbol{\sigma}_1 \cdot \boldsymbol{q})(\boldsymbol{\sigma}_2 \cdot \boldsymbol{q})}{m_{\pi^\pm}^2 + q^2} \frac{\tau_1^+ \tau_2^- + \tau_1^- \tau_2^+}{2} \\
&= -\frac{(\boldsymbol{\sigma}_1 \cdot \boldsymbol{q})(\boldsymbol{\sigma}_2 \cdot \boldsymbol{q})}{m_{\pi^0}^2 + q^2} \boldsymbol{\tau}_1 \cdot \boldsymbol{\tau}_2 + \frac{(\boldsymbol{\sigma}_1 \cdot \boldsymbol{q})(\boldsymbol{\sigma}_2 \cdot \boldsymbol{q})}{m_{\pi^0}^2 + q^2} \frac{\Delta m_\pi^2}{m_{\pi^0}^2 - \Delta m_\pi^2 + q^2} \frac{\tau_1^+ \tau_2^- + \tau_1^- \tau_2^+}{2} \\
&= -\frac{(\boldsymbol{\sigma}_1 \cdot \boldsymbol{q})(\boldsymbol{\sigma}_2 \cdot \boldsymbol{q})}{m_{\pi^0}^2 + q^2} \boldsymbol{\tau}_1 \cdot \boldsymbol{\tau}_2 + \frac{(\boldsymbol{\sigma}_1 \cdot \boldsymbol{q})(\boldsymbol{\sigma}_2 \cdot \boldsymbol{q})}{m_{\pi^0}^2 + q^2} \frac{\Delta m_\pi^2}{m_{\pi^0}^2 - \Delta m_\pi^2 + q^2} (\boldsymbol{\tau}_1 \cdot \boldsymbol{\tau}_2 - \tau_{z1} \tau_{z2}), \tag{A2}
\end{aligned}
$$

where $\tau_j^\pm = \tau_{xj} \pm i\tau_{yj}$ ($j = 1,\ 2$) and $\Delta m_\pi^2 = m_{\pi^0}^2 - m_{\pi^\pm}^2$. The first term of Eq. (A2) corresponds to the isospin symmetric nuclear interaction, while the second term corresponds to the charge-independence breaking one.

APPENDIX B: PRECISE VALUES OF SKYRME PARAMETERS

The precise values of the parameters of SAMi and SAMi-ISB EDFs are shown in Tables VI and VII, respectively. Even though differences of two parameter sets, published and precise, are less than 0.1% level at most, the calculated total energies differ around several hundred keV in SAMi (-1636.1648 MeV by the published parameter set and

-1636.6149 MeV by the precise parameter set for ^{208}Pb) and even several MeV in SAMi-ISB (-1629.2878 MeV by the published parameter set and -1635.6319 MeV by the precise parameter set for ^{208}Pb). Although both parameter sets give similar root-mean-square radii, the results may differ in the order of 0.001 fm level (5.5187 fm by the published SAMi and 5.5185 fm by the precise SAMi, while 5.5092 fm by the published SAMi-ISB and 5.5071 fm by the precise SAMi-ISB for ^{208}Pb). Thus, one needs to use the precise parameter sets to achieve enough accuracy for the present aim, so that we use the precise parameter sets in this paper.

TABLE VI. Parameters of SAMi EDF [59]. Columns named "Published" and "Precise" show the parameters given in the published paper and those with precise values, respectively.

	Published	Precise
t_0 (MeV fm^3)	-1877.75	-1877.746
t_1 (MeV fm^5)	475.6	475.5856
t_2 (MeV fm^5)	-85.2	-85.20021
t_3 (MeV fm$^{3+3\alpha}$)	10219.6	10219.58
x_0	0.320	0.3197176
x_1	-0.532	-0.5319419
x_2	-0.014	-0.0137857
x_3	0.688	0.6883226
W_0 (MeV fm^5)	137	137.0603
W_0' (MeV fm^5)	42	42.32571
α	0.25614	0.2561388

TABLE VII. The same as Table VI but for SAMi-ISB EDF [22].

	Published	Precise
t_0 (MeV fm^3)	-2098.3	-2098.259
t_1 (MeV fm^5)	394.7	394.7479
t_2 (MeV fm^5)	-136.4	-136.4254
t_3 (MeV fm$^{3+3\alpha}$)	11995	11995.53
x_0	0.242	0.2419145
x_1	-0.17	-0.1711566
x_2	-0.470	-0.4702394
x_3	0.32	0.3208390
W_0 (MeV fm^5)	294	294.7846
W_0' (MeV fm^5)	-367	-367.3859
α	0.223	0.2233004
s_0 (MeV fm^3)	-26.3	-26.3
u_0 (MeV fm^3)	25.8	25.8
y_0	-1	-1
z_0	-1	-1

[1] W. Heisenberg, Über den Bau der Atomkerne. I, Z. Phys. **77**, 1 (1932).

[2] S. A. Coon and M. D. Scadron, Two-pion exchange contributions to charge asymmetric and charge dependent nuclear forces, Phys. Rev. C **26**, 2402 (1982).

[3] K. Okamoto, Coulomb energy of He^3 and possible charge asymmetry of nuclear forces, Phys. Lett. **11**, 150 (1964).

[4] J. A. Nolen, Jr. and J. P. Schiffer, Coulomb Energies, Annu. Rev. Nucl. Sci. **19**, 471 (1969).

[5] S. Shlomo, Nuclear Coulomb energies, Rep. Prog. Phys. **41**, 957 (1978).

[6] T. Hatsuda, H. Høgaasen, and M. Prakash, QCD Sum Rules in Medium and the Okamoto-Nolen-Schiffer Anomaly, Phys. Rev. Lett. **66**, 2851 (1991).

[7] H. Sagawa, N. Van Giai, and T. Suzuki, Isospin mixing and the sum rule of super-allowed fermi β decay, Phys. Lett. B **353**, 7 (1995).

[8] B. A. Brown, New Skyrme interaction for normal and exotic nuclei, Phys. Rev. C **58**, 220 (1998).

[9] B. A. Brown, W. A. Richter, and R. Lindsay, Displacement energies with the Skyrme Hartree-Fock method, Phys. Lett. B **483**, 49 (2000).

[10] H. Liang, N. Van Giai, and J. Meng, Isospin corrections for superallowed Fermi β decay in self-consistent relativistic random-phase approximation approaches, Phys. Rev. C **79**, 064316 (2009).

[11] K. Kaneko, S. Tazaki, T. Mizusaki, Y. Sun, M. Hasegawa, and G. de Angelis, Isospin symmetry breaking at high spins in the mirror pair ^{67}Se and ^{67}As, Phys. Rev. C **82**, 061301(R) (2010).

[12] K. Kaneko, T. Mizusaki, Y. Sun, S. Tazaki, and G. de Angelis, Coulomb Energy Difference as a Probe of Isospin-Symmetry Breaking in the Upper fp-Shell Nuclei, Phys. Rev. Lett. **109**, 092504 (2012).

[13] W. Satuła, J. Dobaczewski, W. Nazarewicz, and T. R. Werner, Isospin-breaking corrections to superallowed Fermi β decay in isospin- and angular-momentum-projected nuclear density functional theory, Phys. Rev. C **86**, 054316 (2012).

[14] R. B. Wiringa, S. Pastore, S. C. Pieper, and G. A. Miller, Charge-symmetry breaking forces and isospin mixing in ^{8}Be, Phys. Rev. C **88**, 044333 (2013).

[15] K. Kaneko, Y. Sun, T. Mizusaki, and S. Tazaki, Variation in Displacement Energies Due to Isospin-Nonconserving Forces, Phys. Rev. Lett. **110**, 172505 (2013).

[16] K. Kaneko, Y. Sun, T. Mizusaki, and S. Tazaki, Isospin nonconserving interaction in the $T = 1$ analogue states of the mass-70 region, Phys. Rev. C **89**, 031302(R) (2014).

[17] K. Kaneko, Y. Sun, T. Mizusaki, and S. Tazaki, Probing isospin-symmetry breaking with the modern storage rings and other advanced facilities, Phys. Scr. **2015**, 014011 (2015).

[18] J. C. Hardy and I. S. Towner, Superallowed $0^+ \rightarrow 0^+$ nuclear β decays: 2014 critical survey, with precise results for V_{ud} and CKM unitarity, Phys. Rev. C **91**, 025501 (2015).

[19] K. Kaneko, Y. Sun, T. Mizusaki, S. Tazaki, and S. K. Ghorui, Isospin-symmetry breaking in superallowed Fermi β-decay due to isospin-nonconserving forces, Phys. Lett. B **773**, 521 (2017).

[20] J. M. Dong, Y. H. Zhang, W. Zuo, J. Z. Gu, L. J. Wang, and Y. Sun, Generalized isobaric multiplet mass equation and its application to the Nolen-Schiffer anomaly, Phys. Rev. C **97**, 021301(R) (2018).

[21] K. Kaneko, Y. Sun, and T. Mizusaki, Isoscalar neutron-proton pairing and SU(4)-symmetry breaking in Gamow-Teller transitions, Phys. Rev. C **97**, 054326 (2018).

[22] X. Roca-Maza, G. Colò, and H. Sagawa, Nuclear Symmetry Energy and the Breaking of the Isospin Symmetry: How Do They Reconcile with Each Other? Phys. Rev. Lett. **120**, 202501 (2018).

[23] B. M. Loc, N. Auerbach, and G. Colò, Isospin mixing and Coulomb mixing in ground states of even-even nuclei, Phys. Rev. C **99**, 014311 (2019).

[24] J. M. Dong, J. Z. Gu, Y. H. Zhang, W. Zuo, L. J. Wang, Y. A. Litvinov, and Y. Sun, Beyond Wigner's isobaric multiplet mass equation: Effect of charge-symmetry-breaking interaction and Coulomb polarization, Phys. Rev. C **99**, 014319 (2019).

[25] X. Roca-Maza, H. Sagawa, and G. Colò, Double charge-exchange phonon states, Phys. Rev. C **101**, 014320 (2020).

[26] S. J. Novario, D. Lonardoni, S. Gandolfi, and G. Hagen, Trends of Neutron Skins and Radii of Mirror Nuclei from First Principles, Phys. Rev. Lett. **130**, 032501 (2023).

[27] G. Selva, X. Roca-Maza, and G. Colò, Isospin Symmetry Breaking Effects on the Mass-Radius Relation of a Neutron Star, Symmetry **13**, 144 (2021).

[28] N. Auerbach, Coulomb effects in nuclear structure, Phys. Rep. **98**, 273 (1983).

[29] T. Naito, R. Akashi, and H. Liang, Application of a Coulomb energy density functional for atomic nuclei: Case studies of local density approximation and generalized gradient approximation, Phys. Rev. C **97**, 044319 (2018).

[30] T. Naito, X. Roca-Maza, G. Colò, and H. Liang, Coulomb exchange functional with generalized gradient approximation for self-consistent Skyrme Hartree-Fock calculations, Phys. Rev. C **99**, 024309 (2019).

[31] T. Naito, X. Roca-Maza, G. Colò, and H. Liang, Effects of finite nucleon size, vacuum polarization, and electromagnetic spin-orbit interaction on nuclear binding energies and radii in spherical nuclei, Phys. Rev. C **101**, 064311 (2020).

[32] D. Vautherin and D. M. Brink, Hartree-Fock Calculations with Skyrme's Interaction. I. Spherical Nuclei, Phys. Rev. C **5**, 626 (1972).

[33] P. Bączyk, J. Dobaczewski, M. Konieczka, W. Satuła, T. Nakatsukasa, and K. Sato, Isospin-symmetry breaking in masses of $N \simeq Z$ nuclei, Phys. Lett. B **778**, 178 (2018).

[34] P. Bączyk, W. Satuła, J. Dobaczewski, and M. Konieczka, Isobaric multiplet mass equation within nuclear density functional theory, J. Phys. G **46**, 03LT01 (2019).

[35] P. Bączyk and W. Satuła, Mirror energy differences in $T = 1/2$ $f_{7/2}$-shell nuclei within isospin-dependent density functional theory, Phys. Rev. C **103**, 054320 (2021).

[36] T. Naito, G. Colò, H. Liang, X. Roca-Maza, and H. Sagawa, Toward *ab initio* charge symmetry breaking in nuclear energy density functionals, Phys. Rev. C **105**, L021304 (2022).

[37] T. Naito, X. Roca-Maza, G. Colò, H. Liang, and H. Sagawa, Isospin symmetry breaking in the charge radius difference of mirror nuclei, Phys. Rev. C **106**, L061306 (2022).

[38] U. C. Perera, A. V. Afanasjev, and P. Ring, Charge radii in covariant density functional theory: A global view, Phys. Rev. C **104**, 064313 (2021).

[39] W. D. Myers and W. J. Swiatecki, Average nuclear properties, Ann. Phys. (NY) **55**, 395 (1969).

[40] X. Roca-Maza, M. Centelles, X. Viñas, and M. Warda, Neutron Skin of ^{208}Pb, Nuclear Symmetry Energy, and the Parity Radius Experiment, Phys. Rev. Lett. **106**, 252501 (2011).

[41] P.-G. Reinhard and W. Nazarewicz, Information content of the differences in the charge radii of mirror nuclei, Phys. Rev. C **105**, L021301 (2022).

[42] T. H. R. Skyrme, The effective nuclear potential, Nucl. Phys. **9**, 615 (1958).

[43] X. Roca-Maza and N. Paar, Nuclear equation of state from ground and collective excited state properties of nuclei, Prog. Part. Nucl. Phys. **101**, 96 (2018).

[44] G. A. Miller, A. K. Opper, and E. J. Stephenson, Charge Symmetry Breaking and QCD, Annu. Rev. Nucl. Part. Sci. **56**, 253 (2006).

[45] M. V. Stoitsov, J. Dobaczewski, W. Nazarewicz, and P. Ring, Axially deformed solution of the Skyrme-Hartree-Fock-Bogolyubov equations using the transformed harmonic oscillator basis. The program HFBTHO (v1.66p), Comput. Phys. Commun. **167**, 43 (2005).

[46] K. Sato, J. Dobaczewski, T. Nakatsukasa, and W. Satuła, Energy-density-functional calculations including proton-neutron mixing, Phys. Rev. C **88**, 061301(R) (2013).

[47] J. A. Sheikh, N. Hinohara, J. Dobaczewski, T. Nakatsukasa, W. Nazarewicz, and K. Sato, Isospin-invariant Skyrme energy-density-functional approach with axial symmetry, Phys. Rev. C **89**, 054317 (2014).

[48] J. Dobaczewski, P. Bączyk, P. Becker, M. Bender, K. Bennaceur, J. Bonnard, Y. Gao, A. Idini, M. Konieczka, M. Kortelainen, L. Próchniak, A. M. Romero, W. Satuła, Y. Shi, T. R. Werner, and L. F. Yu, Solution of universal nonrelativistic nuclear DFT equations in the Cartesian deformed harmonic-oscillator basis. (IX) HFODD (v3.06h): A new version of the program, J. Phys. G **48**, 102001 (2021).

[49] H. Sagawa, G. Colò, X. Roca-Maza, and Y. Niu, Collective excitations involving spin and isospin degrees of freedom, Eur. Phys. J. A **55**, 227 (2019).

[50] P.-G. Reinhard, D. J. Dean, W. Nazarewicz, J. Dobaczewski, J. A. Maruhn, and M. R. Strayer, Shape coexistence and the effective nucleon-nucleon interaction, Phys. Rev. C **60**, 014316 (1999).

[51] P. Danielewicz and J. Lee, Symmetry energy I: Semi-infinite matter, Nucl. Phys. A **818**, 36 (2009).

[52] C. Mondal, B. K. Agrawal, J. N. De, and S. K. Samaddar, Correlations among symmetry energy elements in Skyrme models, Int. J. Mod. Phys. E **27**, 1850078 (2018).

[53] P. Hohenberg and W. Kohn, Inhomogeneous electron gas, Phys. Rev. **136**, B864 (1964).

[54] W. Kohn and L. J. Sham, Self-consistent equations including exchange and correlation effects, Phys. Rev. **140**, A1133 (1965).

[55] W. Kohn, Nobel Lecture: Electronic structure of matter—wave functions and density functionals, Rev. Mod. Phys. **71**, 1253 (1999).

[56] M. Bender, P.-H. Heenen, and P.-G. Reinhard, Self-consistent mean-field models for nuclear structure, Rev. Mod. Phys. **75**, 121 (2003).

[57] J. Meng, H. Toki, S. G. Zhou, S. Q. Zhang, W. H. Long, and L. S. Geng, Relativistic continuum Hartree Bogoliubov theory for ground-state properties of exotic nuclei, Prog. Part. Nucl. Phys. **57**, 470 (2006).

[58] H. Liang, J. Meng, and S.-G. Zhou, Hidden pseudospin and spin symmetries and their origins in atomic nuclei, Phys. Rep. **570**, 1 (2015).

[59] X. Roca-Maza, G. Colò, and H. Sagawa, New Skyrme interaction with improved spin-isospin properties, Phys. Rev. C **86**, 031306(R) (2012).

[60] X. Roca-Maza, M. Brenna, B. K. Agrawal, P. F. Bortignon, G. Colò, L.-G. Cao, N. Paar, and D. Vretenar, Giant quadrupole resonances in ^{208}Pb, the nuclear symmetry energy, and the neutron skin thickness, Phys. Rev. C **87**, 034301 (2013).

[61] A. Bulgac and V. R. Shaginyan, A systematic surface contribution to the ground-state binding energies, Nucl. Phys. A **601**, 103 (1996).

[62] A. Bulgac and V. R. Shaginyan, Influence of Coulomb correlations on the location of drip line, single particle spectra and effective mass, Eur. Phys. J. A **5**, 247 (1999).

[63] A. Bulgac and V. R. Shaginyan, Proton single-particle energy shifts due to Coulomb correlations, Phys. Lett. B **469**, 1 (1999).

[64] P. A. M. Dirac, Note on exchange phenomena in the thomas atom, Math. Proc. Camb. Phil. Soc. **26**, 376 (1930).

[65] J. C. Slater, A simplification of the Hartree-Fock method, Phys. Rev. **81**, 385 (1951).

[66] J. P. Perdew, K. Burke, and M. Ernzerhof, Generalized Gradient Approximation Made Simple, Phys. Rev. Lett. **77**, 3865 (1996).

[67] J. Friedrich and T. Walcher, A coherent interpretation of the form factors of the nucleon in terms of a pion cloud and constituent quarks, Eur. Phys. J. A **17**, 607 (2003).

[68] G. Colò, L. Cao, N. Van Giai, and L. Capelli, Self-consistent RPA calculations with Skyrme-type interactions: The skyrme_rpa program, Comput. Phys. Commun. **184**, 142 (2013).

[69] B. A. Brown, Neutron Radii in Nuclei and the Neutron Equation of State, Phys. Rev. Lett. **85**, 5296 (2000).

[70] L.-W. Chen, C. M. Ko, and B.-A. Li, Nuclear matter symmetry energy and the neutron skin thickness of heavy nuclei, Phys. Rev. C **72**, 064309 (2005).

[71] J. Zenihiro, H. Sakaguchi, S. Terashima, T. Uesaka, G. Hagen, M. Itoh, T. Murakami, Y. Nakatsugawa, T. Ohnishi, H. Sagawa, H. Takeda, M. Uchida, H. P. Yoshida, S. Yoshida, and M. Yosoi, Direct determination of the neutron skin thicknesses in ^{40,48}Ca from proton elastic scattering at $E_p = 295$ MeV, arXiv:1810.11796 [nucl-ex].

[72] D. Adhikari, H. Albataineh, D. Androic, K. A. Aniol, D. S. Armstrong, T. Averett, C. Ayerbe Gayoso, S. K. Barcus, V. Bellini, R. S. Beminiwattha, J. F. Benesch, H. Bhatt, D. Bhatta Pathak, D. Bhetuwal, B. Blaikie, J. Boyd, Q. Campagna, A. Camsonne, G. D. Cates, Y. Chen *et al.* (CREX Collaboration), Precision Determination of the Neutral Weak Form Factor of ^{48}Ca, Phys. Rev. Lett. **129**, 042501 (2022).

[73] J. Zenihiro, H. Sakaguchi, T. Murakami, M. Yosoi, Y. Yasuda, S. Terashima, Y. Iwao, H. Takeda, M. Itoh, H. P. Yoshida, and M. Uchida, Neutron density distributions of ^{204,206,208}Pb deduced via proton elastic scattering at $E_p = 295$ MeV, Phys. Rev. C **82**, 044611 (2010).

[74] D. Adhikari, H. Albataineh, D. Androic, K. Aniol, D. S. Armstrong, T. Averett, C. Ayerbe Gayoso, S. Barcus, V. Bellini, R. S. Beminiwattha, J. F. Benesch, H. Bhatt, D. Bhatta Pathak, D. Bhetuwal, B. Blaikie, Q. Campagna, A. Camsonne, G. D. Cates, Y. Chen, C. Clarke *et al.* (PREX Collaboration), Accurate Determination of the Neutron Skin Thickness of ^{208}Pb through

Parity-Violation in Electron Scattering, Phys. Rev. Lett. **126**, 172502 (2021).

[75] P.-G. Reinhard, X. Roca-Maza, and W. Nazarewicz, Information Content of the Parity-Violating Asymmetry in ^{208}Pb, Phys. Rev. Lett. **127**, 232501 (2021).

[76] M. Baldo and G. F. Burgio, The nuclear symmetry energy, Prog. Part. Nucl. Phys. **91**, 203 (2016).

[77] I. Hamamoto and H. Sagawa, Gamow-Teller beta decay and isospin impurity in nuclei near the proton drip line, Phys. Rev. C **48**, R960 (1993).

[78] H. Sagawa, N. Van Giai, and T. Suzuki, Effect of isospin mixing on superallowed Fermi β decay, Phys. Rev. C **53**, 2163 (1996).

[79] H. Sagawa, S. Yoshida, T. Naito, T. Uesaka, J. Zenihiro, J. Tanaka, and T. Suzuki, Isovector density and isospin impurity in ^{40}Ca, Phys. Lett. B **829**, 137072 (2022).

[80] M. Centelles, X. Roca-Maza, X. Viñas, and M. Warda, Origin of the neutron skin thickness of ^{208}Pb in nuclear mean-field models, Phys. Rev. C **82**, 054314 (2010).

[81] S. Goriely and J. M. Pearson, Further explorations of Skyrme-Hartree-Fock-Bogoliubov mass formulas. VIII. Role of Coulomb exchange, Phys. Rev. C **77**, 031301(R) (2008).

[82] C. J. Horowitz and J. Piekarewicz, Impact of spin-orbit currents on the electroweak skin of neutron-rich nuclei, Phys. Rev. C **86**, 045503 (2012).

[83] P.-G. Reinhard and W. Nazarewicz, Nuclear charge densities in spherical and deformed nuclei: Toward precise calculations of charge radii, Phys. Rev. C **103**, 054310 (2021).

[84] T. Naito, G. Colò, H. Liang, and X. Roca-Maza, Second and fourth moments of the charge density and neutron-skin thickness of atomic nuclei, Phys. Rev. C **104**, 024316 (2021).

[85] I. Angeli and K. P. Marinova, Table of experimental nuclear ground state charge radii: An update, At. Data Nucl. Data Tables **99**, 69 (2013).

[86] W. J. Huang, M. Wang, F. Kondev, G. Audi, and S. Naimi, The AME 2020 atomic mass evaluation (I). Evaluation of input data, and adjustment procedures, Chin. Phys. C **45**, 030002 (2021).

[87] P.-G. Reinhard and W. Nazarewicz, Toward a global description of nuclear charge radii: Exploring the Fayans energy density functional, Phys. Rev. C **95**, 064328 (2017).

[88] X. Viñas, M. Centelles, X. Roca-Maza, and M. Warda, Density dependence of the symmetry energy from neutron skin thickness in finite nuclei, Eur. Phys. J. A **50**, 27 (2014).

[89] H. Sotani, N. Nishimura, and T. Naito, New constraints on the neutron-star mass and radius relation from terrestrial nuclear experiments, Prog. Theor. Exp. Phys. **2022**, 041D01 (2022).

[90] H. Yukawa, On the interaction of elementary particles. I, Proc. Phys. Math. Soc. Jpn. Third **17**, 48 (1935).

[91] R. Machleidt, K. Holinde, and C. Elster, The Bonn meson-exchange model for the nucleon–nucleon interaction, Phys. Rep. **149**, 1 (1987).